Quantification of morphological, functional, and biochemical features of H9c2 rat cardiomyoblast retinoic acid differentiation

Nicole S. York[1], Joel E. Rivera[1], Mohammadreza Rahmani Manesh[1], K'sana Wood Lynes-Ford[1,2], Rory Smith[1], Leigh E. Wicki-Stordeur[1], Laura T. Arbour[1,2,3], Leigh Anne Swayne[1,3*]

(1) Division of Medical Sciences, University of Victoria, Victoria, British Columbia, Canada
(2) Department of Medical Genetics, University of British Columbia, Victoria, British Columbia, Canada
(3) Island Medical Program, University of British Columbia, Victoria, British Columbia, Canada

(*) Correspondence should be addressed to Leigh Anne Swayne, lswayne@uvic.ca or to Nicole York, nicoleyork@uvic.ca.

Running Head: Quantification of H9c2 cell differentiation

Abbreviations:

iPSC	induced pluripotent stem cell
$Ca_v1.2$	protein pore subunit of the of the L-type calcium channel encoded by the *CACNA1C* gene
Ca^{2+}	Calcium ions
$[Ca^{2+}]_i$	Internal calcium ion concentration
STED	Stimulated emission depletion
NaCl	Sodium chloride
E15.5	Embryonic Day 15.5
P2	Postnatal Day 2
DMEM	Dulbecco's Modified Eagle Medium
FBS	Fetal bovine serum
RIPA	Radio-Immunoprecipitation Assay
BDM	2,3-Butanedione monoxime
HBSS	Hanks' Balanced Salt Solution
dPBS	Dulbecco's Phosphate-Buffered Saline
Sqrt	Square root
FOV	field of view
FC	fold change
TBS	Tris-buffered saline
TBS-T	Tris-buffered saline, 0.1% Tween-20

Abstract

Cell culture models enable advancement in our understanding of heart development and heart disease. The H9c2 rat ventricular cardiomyoblast cell line can be differentiated, recapitulating certain components of cardiomyocyte development; however, morphological, functional, and biochemical changes are rarely investigated in parallel, thereby limiting fulsome understanding. We therefore characterized morphology, Ca^{2+} handling, and gene expression after five days (5 *days-in-vitro*, DIV5), and fourteen days (DIV14) of exposure to differentiation stimuli, consisting of retinoic acid and low serum. We observed several morphological changes with increasing time in differentiation, including increased mean length, area, eccentricity, and multinucleation, as well as an increase in actin clusters. Spontaneous Ca^{2+} transients in differentiated H9c2 cells had decreased frequency and synchronicity compared to those observed in primary cardiomyocytes. Additionally, key cardiomyocyte cytoskeletal proteins and ion channel transcript and protein expression levels changed significantly with differentiation, in alignment with changes normally observed in cardiomyocyte development. Our findings suggest H9c2 cells may be used as a high throughput screening model to investigate cardiomyocyte biology in certain developmental contexts with relevance to heart health and disease.

Key words

H9c2, differentiation, retinoic acid, morphology, spontaneous calcium transients

Highlights

42

43 - We quantified morphology, Ca^{2+} handling, and gene expression changes in rat
44 ventricular cardiomyoblast H9c2 cells across retinoic acid differentiation.
45 - We compared multiple differentiation time points (mainly DIV0, DIV5, and DIV14) and
46 observed time-dependent changes in all 3 aspects. We observed several
47 morphological changes with increasing time in differentiation, including increased
48 mean length, area, eccentricity, and multinucleation, as well as an increase in actin
49 clusters. We observed the onset of spontaneous Ca^{2+} transients with differentiation,
50 with further changes in subpopulations with increasing time in differentiation. Finally,
51 we observed multiple changes in gene expression consistent with cardiomyocyte
52 differentiation.
53 - We summarize these parallel time-point dependent changes in morphology, Ca^{2+}
54 handing, and gene expression to enable other researchers to optimize their study
55 design.

56

57 **Introduction**

58 Cardiomyocyte-like cell culture models, including immortalized cell lines such as the
59 H9c2 rat ventricular cardiomyoblast cell line, human induced pluripotent stem cell (iPSC)-
60 derived cardiomyocytes, and rodent primary cardiomyocyte cultures play key,
61 complementary roles in modeling cardiomyocyte development. Together, their
62 coordinated use could enable fulsome modelling of the cellular changes in health and
63 disease contexts. Each of these models has key strengths and weaknesses facilitating the

64 study of different aspects of cardiomyocyte development and viability. The H9c2
65 cardiomyoblast cell line can be differentiated with low serum and retinoic acid to express
66 phenotypes associated with cardiomyocytes [1–3]. As an immortalized cell line, H9c2 cells
67 convenient to work with, suggest retinoic acid-differentiated H9c2 cells could be an
68 attractive model to study aspects of cardiomyoblast and/or cardiomyocyte biology (Figure
69 1). However, there remain significant gaps in the quantitative changes in these cells across
70 different cellular parameters altered by differentiation, that hinder their use. To this we
71 measured changes in H9c2 cell morphology, Ca2+ handling, and gene expression across
72 retinoic acid differentiation, to better enable their use as a model for cardiomyoblast
73 and/or cardiomyocyte biology in health and disease contexts.
74 The H9c2 cell line was first isolated from the lower half of a rat ventricle at
75 embryonic day 13 [4]. Following selective passage to enrich for cardiomyoblasts, the cells
76 ceased beating but maintained other key cardiomyoblast characteristics [4], such as their
77 morphology, ultrastructure, and presence of specific ion channels [1,4–6]. Early work
78 showed that retinoic acid differentiation increased $Ca_v1.2$ (α_{1C})-based L-type Ca^{2+} channel
79 expression [1], which are enriched in and important for generating the electrical and
80 mechanical properties of cardiomyocytes [7], and cardiac troponins [2]. Several additional
81 studies have investigated the morphological and biochemical aspects of differentiated
82 H9c2 cells [2,3], but functional studies are rare [1,8]. H9c2 cell differentiation is
83 associated with elongation of cell shape [3,6–8], but this has not been fully quantified [1–
84 4].

85 Consequently, the amplitude and extent of changes in basic morphological
86 properties associated with differentiation is unclear. To date, characterization of H9c2 cell
87 intracellular Ca^{2+} handling has been limited to stimulation of undifferentiated cells [8–10],
88 but the impact of differentiation on baseline H9c2 cell Ca^{2+} handling properties is
89 unknown. H9c2 cell differentiation is associated with increased expression of genes
90 encoding cardiomyocyte markers, such as cardiac troponins, and genes involved in Ca^{2+}
91 handling and mitochondrial metabolism [2]**.** Although H9c2 cell differentiation-associated
92 gene expression changes are better defined [2,3,8], they have rarely been compared with
93 morphological and/or functional aspects in parallel. Furthermore, early changes (e.g., 5
94 hours to 3 days), which could be driving various signaling processes, have not been
95 thoroughly investigated. The amplitude and timing of gene expression changes relative to
96 morphological and Ca2+ handling changes is rarely studied in parallel, making it difficult to
97 identify possible connections.
98 To this end, we quantified morphology, Ca^{2+} handling, and gene expression changes
99 across H9c2 cell retinoic acid differentiation in parallel, comparing mainly three time
100 points, DIV0, DIV5, and DIV14. We used confocal and super-resolution microscopy,
101 intracellular Ca^{2+} imaging, as well as RT-qPCR and Western blotting to assess these
102 changes. We observed several morphological changes with increasing time in
103 differentiation, including increased mean length, area, eccentricity, and multinucleation,
104 as well as an increase in actin clusters. We observed the onset of spontaneous Ca^{2+}
105 transients with differentiation, with further changes in subpopulations with increasing time
106 in differentiation. We also observed multiple changes in gene expression consistent with

107 cardiomyocyte differentiation, such as increased *Myom2*, *Cacna1c*, GATA4, and cTnT
108 expression. Finally, we compiled and summarize these changes according to DIV to enable
109 optimal use of differentiated H9c2 cells in modelling aspects of cardiomyoblast and/or
110 cardiomyocytes in health and disease contexts.
111

112 **Results**

113 **Differentiated H9c2 cells become larger, multi-nucleated, and develop localized actin**
114 **intensities**

115 During cardiomyocyte differentiation, cells undergo changes in their overall shape
116 that are key for their function [11–13]. Prior work commonly differentiated H9c2 cells up to
117 DIV5 [2,3] yet more recent work has extended differentiation to DIV14 [8]. We compared an
118 array of gross morphology features of undifferentiated (DIV0), DIV5- and DIV14-
119 differentiated H9c2 cells by analyzing confocal images of F-actin (phalloidin) and nuclei
120 (Hoechst) (Figure 2A) with a custom MATLAB script (available on github), refer to Table 1 for
121 statistical analyses. Average cell length was significantly greater at DIV14 compared to
122 DIV0, with corresponding right shifts in the frequency distribution plot of cell length for
123 both DIV5 and DIV14 cell populations (Figure 2Bi, Ci). Cell area also significantly increased
124 at DIV14 compared to both DIV0 and DIV5 cells, and the frequency distribution plot of cell
125 area exhibited right shifts for both DIV5 and DIV14 cell populations (Figure 2Bii, Cii). Cell
126 eccentricity increased at DIV5 compared to DIV0, with no further change evident at DIV14
127 (Figure 2Biii). Corresponding right shifts were evident in the frequency distribution plot of
128 cell eccentricity for both DIV5 and DIV14 cell populations (Figure 2Ciii). The proportion of

129 multinucleated cells was also drastically increased at DIV14 compared to DIV0 (Figure
130 2Biv, Civ). We found no significant changes in mean cell perimeter across differentiation,
131 however the frequency distribution plot for cell perimeter did show some right shifting of
132 DIV5 and DIV14 cell populations (Figure S1). Together these data indicate that
133 differentiated H9c2 cells are, on average, longer, larger, more eccentric (less circular) and
134 more likely to be multinucleated than undifferentiated DIV0 cells. Moreover, these
135 changes are more apparent at the DIV14 differentiation timepoint than at DIV5, suggesting
136 that extending the differentiation time course further enhances cardiomyocyte-like
137 phenotypic changes.

138 Notably, we observed that DIV14 differentiated H9c2 cells commonly exhibited
139 localized actin intensities, or "clusters" of F-actin (phalloidin+) (Figure 2Aiii) like those
140 previously reported in other cell types [14–16]. We used stimulated emission depletion
141 (STED) super-resolution microscopy to further resolve these F-actin clusters, which were
142 circular to ellipsoid in nature (Figure 2D). At DIV14, 61.8% ± 5.1 of cells showed actin
143 clusters compared to 10.8% ± 2.0 of cells at DIV5 (unpaired t-test, $p<0.0001$; Figure 2Ei).
144 Of the cells that exhibited actin clusters, the average number of clusters per cell increased
145 between these time points (DIV5, 1.0 ± 0.1 clusters/cell *vs*. DIV14, 2.7 ± 0.3 clusters/cell;
146 unpaired t-test, $p<0.0001$; Figure 2Eii).

147 Together these results suggest that retinoic acid differentiation increases cell
148 length, cell area, eccentricity, and the proportion of multinucleated cells, and induces the
149 formation of circular/elliptical F-actin clusters.

150

151 **Differentiated H9c2 cells develop spontaneous Ca^{2+} transients similar in amplitude to**

152 **primary cardiomyocytes**

153 Intracellular Ca^{2+} handling changes dynamically across the development of

154 cardiomyoblasts into cardiomyocytes [17,18]. But Ca^{2+} handling during H9c2 cell

155 differentiation has not been thoroughly characterized, making it difficult to begin to relate

156 changes in morphology and gene expression to functional outcomes. To this end, with live

157 confocal imaging of Fluo4-AM [19] and previously published MATLAB scripts [20], we

158 examined spontaneous Ca^{2+} transients in undifferentiated and differentiated H9c2 cells

159 and compared DIV5 and DIV14 differentiated H9c2 cells with neonatal primary mouse

160 cardiomyocytes (Figure 3A). At DIV0 we did not observe readily detectable spontaneous

161 Ca^{2+} transients (not shown) and therefore, DIV0 was not included in subsequent analyses.

162 To determine the extent to which differentiation brings H9c2 cells towards

163 cardiomyocytes' Ca^{2+} handling, all metrics were compared to those of primary

164 cardiomyocytes. Mean transient (spike) amplitudes (change in fluorescence from baseline

165 to peak) of all H9c2 cell differentiation conditions were similar to primary cardiomyocytes

166 (Figure 3Bi, Table 2). However, mean spike frequency (spikes per minute) and

167 synchronicity (number of spikes occurring at the same time that exceed a threshold based

168 off the mean intensity profile in all the cells in the field of view (FOV)) were significantly

169 lower in all differentiated H9c2 cell conditions compared to primary cardiomyocytes

170 (Figure 3Bii,iii, Table 2). Distribution plots of frequency and synchronicity data displayed

171 right shifts of the DIV14 population compared to DIV5, suggesting a further shift of DIV14

172 cells closer to the primary cardiomyocyte phenotype.

173 Together these results suggest that spontaneous Ca^{2+} transients develop with
174 differentiation of H9c2 cells and are comparable in amplitude to those of primary
175 cardiomyocytes. Notably, while the longer differentiation timepoint (DIV14) does not
176 overtly alter H9c2 cell Ca^{2+} transients compared to the DIV5 timepoint, there may be
177 subpopulations of DIV14 cells that are shifted closer towards a primary cardiomyocyte-like
178 phenotype.
179
180 **Differentiated H9c2 cells exhibit gene expression changes consistent with**
181 **cardiomyocyte differentiation**
182 In parallel to our assessment of changes in H9c2 cell morphology and Ca^{2+} handling
183 associated with differentiation, we probed transcript (RT-qPCR) and protein (Western
184 blotting) expression levels of genes involved in transcription, cytoskeleton, ion flux
185 regulation, and signal transduction (Figure 4A, see Table S1 for brief descriptions of
186 functions and references). Many of these gene expression changes have been previously
187 described in H9c2 cell differentiation (Rbp2, Tnnt2, Myom2, Pde4a [2]). We also looked at
188 additional gene expression changes based on the cardiomyocyte literature (Nkx2.5, α-
189 actinin). For select transcript changes we confirmed protein expression with Western
190 blotting (cTnT, GATA4, Nkx2.5, β-actin, Cx43, vimentin), and in some cases used only used
191 Western blotting (α-actinin, vinculin, ankyrin-B). We used two types of comparisons. In the
192 first approach, to identify increases or decreases in gene expression associated with H9c2
193 cell differentiation, we quantified the levels of select transcripts and proteins at DIV0,
194 DIV5h, DIV3, DIV5, and DIV14 of retinoic acid differentiation. In the second approach we

195 compared the extent to which the expression levels of select targets in differentiated H9c2
196 cells (DIV5 & DIV14) compare with those of primary cardiomyocytes. Refer to Table 3 for
197 details of fold change results and statistical analyses.

198 We confirmed retinoic acid signaling pathway activation, observing an increase in
199 *Tgm2* (encodes for transglutaminase 2), at DIV5 compared to both DIV0 and DIV5h (Figure
200 4 Bi). Both *Myom2* (encodes for myomesin 2) and *Cacna1c* (encodes for L-type Ca^{2+}
201 channel pore) also observed increased transcript levels, *Myom2* were elevated ~18-fold ~5
202 fold at DIV5 compared to both DIV0 and DIV5h, respectively (Figure 4 Bii, iii). *Gja5* (encodes
203 for connexin43 (Cx43)) levels observed decreased levels at DIV3 and DIV5 (Figure 4 Biv)

204 We further evaluated protein expression changes for Cx43, as well as additional
205 targets (Nkx2.5, GATA4, α-actinin, Cx43, cTnT, vinculin, vimentin, β-actin, ankyrin-B) as
206 shown in Figure 4 Ci, statistical analyses are in Table 4. Both transcription factors, Nkx2.5
207 and GATA4 levels were altered across differentiation (Figure 4 Cii). While Nkx2.5 levels
208 decreased from DIV0 to DIV5, GATA4 levels increased. We also analyzed multiple
209 cytoskeletal proteins (Figure 4 Ciii). Vinculin levels initially increased at DIV5h and DIV3. α-
210 actinin levels decreased at DIV3 and vimentin levels decreased at both DIV3 and DIV5.
211 Ankyrin-B levels increased at DIV3 and DIV5. cTnT levels were increased at DIV5 as well.
212 Lastly, Cx43 levels decreased during H9c2 cell differentiation at both DIV3 and DIV5.

213 Next, to determine which differentiation timepoint best approximates the primary
214 cardiomyocyte phenotype at a gene expression level, we compared the levels of select
215 targets from DIV5 or DIV14 differentiated H9c2 cells to those in cardiomyocytes (Figure 5
216 A). There were no significant differences between DIV5, DIV14, or primary cardiomyocyte

217 transcript expression for any of the genes we analyzed (see Figure 5 A for the list of genes).
218 For analysis of protein levels, we included embryonic (E15.5) and early postnatal (P2)
219 mouse heart tissue samples as positive controls (Figure 5 Bi). Vinculin, α-actinin, and
220 vimentin levels at DIV5 but not DIV14 were significantly different from primary
221 cardiomyocytes (Figure 5 Bii). While the levels of cTnT and Nkx2.5 at both DIV5 and DIV14
222 were significantly reduced in H9c2 cells compared to primary cardiomyocyte levels (Figure
223 5 Bii, Biii)
224 Together, these data are in line with many previously reported changes in the
225 expression of several key ion channels and cytoskeleton-associated genes with H9c2 cell
226 differentiation alters, and identify several new ones, including α-actinin and ankyrin-B.
227 Overall, these results suggest DIV14 cells most closely resemble the primary
228 cardiomyocyte gene expression.
229
230 **Summary of major changes and associated experimental recommendations**
231 The use of H9c2 cells across different timepoints, DIV0-3, DIV5, and DIV14, may be
232 useful for different studies depending on the research question. H9c2 cells at DIV0
233 represent the undifferentiated baseline, with smaller, mononucleated cells lacking
234 calcium signaling and with decreased expression of several key cardiomyocyte genes (e.g.,
235 *Myom2, Cacna1c*, cTnT). For detecting early changes to gene expression timepoints before
236 DIV5 may be of use (such as DIV5h or DIV3). DIV5 cells highlight initial changes to cell
237 eccentricity and trends towards cell shape changes, the emergence of spontaneous Ca^{2+}
238 transients, and gene expression changes associated with mature cardiomyocytes. By

239 DIV14, cells exhibit pronounced cardiomyocyte-like features, such as multinucleation,
240 actin clusters, Ca^{2+} handling, and gene profiles more closely resembling primary
241 cardiomyocytes. H9c2 cells at DIV14 are likely the best candidate for morphological and
242 functional outputs while DIV5 and earlier cells are beneficial for studying gene expression
243 changes preceding the morphological changes.
244

245 **Discussion**

246 Here we conducted a parallel analysis of H9c2 cell morphology, spontaneous Ca^{2+}
247 handling, and gene expression over retinoic acid differentiation. We found that
248 differentiated H9c2 cells recapitulate specific aspects of cardiomyocyte differentiation in
249 all three areas, as summarized in Figure 1. This information will facilitate the optimal use of
250 differentiated H9c2 cells to advance understanding of the mechanisms underlying
251 cardiomyocyte differentiation with health and disease applications.

252 Our quantitative analysis of H9c2 cell morphology revealed marked changes in
253 multiple aspects across H9c2 cell differentiation. These include increases in mean area,
254 eccentricity, and multinucleation (Figure 2). The most robust morphological differences
255 were observed at DIV14, expanding upon the findings observed by others [3,8] by
256 incorporating additional measures including quantifying length, perimeter, and
257 eccentricity in addition to area and multinucleation. These findings suggest that DIV14 is
258 the best model for investigating elements related to morphology and function. Early gene
259 expression changes related to cytoskeletal organization. Such as upregulation increased
260 expression of *Cacna1c*, which encodes for the L-type Ca^{2+} channel pore, not only initiates

261 Ca^{2+} signaling but also supports downstream calcium-dependent cytoskeletal remodeling
262 pathways. Modulation of proteins like vinculin, α-actinin, vimentin, and ankyrin-B, likely
263 contribute to the increases in cell length, area, and eccentricity observed across
264 differentiation. These structural changes are further accompanied by the emergence of
265 actin clusters, which became significantly more prevalent at DIV14, as revealed by super-
266 resolution microscopy (Figure 2 D,E). Changes in actin are key for the development of
267 cardiomyocyte cell shape and sarcomere formation [21–23] and while the role of actin
268 clusters has not been thoroughly characterized in cardiomyocytes, they are known to play
269 important roles in regulating actin dynamics in other cell types [24–26]. Therefore,
270 differentiated H9c2 cells could provide a model in which to investigate the generation and
271 role of actin clusters in cardiomyocyte development. Spontaneous Ca^{2+} transients first
272 appeared at DIV5 (Figure 3), aligning with early increases in calcium-handling gene
273 expression, such as *Cacna1c*. Although average Ca^{2+} dynamics in H9c2 cells did not reach
274 primary cardiomyocyte levels, distribution shifts at DIV14 more closely resemble the
275 dynamics of primary cardiomyocytes compared to DIV5. The morphological changes,
276 presence of spontaneous Ca^{2+} transients, and gene expression changes at DIV14 the most
277 suitable to model cardiomyocytes.
278
279 **Translational implications**
280 The ability of differentiated H9c2 cells to model key morphological, functional, and gene
281 expression features of cardiomyocytes highlights their relevance as a model system for
282 investigating the cellular and molecular mechanisms underlying cardiac development and

283 disease. While this differentiation is nuanced, the ability to model cardiomyocyte
284 differentiation in a robust and easily manipulated cell line allows for experiments including
285 prioritizing hypotheses before advancing to more complex models and high throughput
286 screenings of therapeutics. Furthermore, the ease of transfection and use of inducible
287 vectors enables the investigation of the impacts of genetic variants at various stages of
288 cardiomyocyte differentiation (Figure S2). Overall, the morphological, functional, and gene
289 expression changes that occur across differentiation indicate that H9c2 cells are useful for
290 identifying disease mechanisms, therapeutic targets, and developing interventions.
291
292 **Limitations**
293 One of the challenges in measuring the morphology of H9c2 cells is the proximity of
294 cells; however, this feature itself is a critical process during cardiomyocyte development
295 and in diseased states [27,28]. As a result, the segmentation was challenging given the
296 strong expression of actin stress fibers throughout the cell. To measure the morphology of
297 H9c2 cells we identified the number of segmentable cells (cells with clear boundaries) in
298 an FOV and randomly selected 3 cells. Inherently, this may have favoured the more
299 undifferentiated cells in the FOV as they are less aligned by nature. Future studies could
300 employ cell perimeter stains such as wheat germ agglutinin for easier analysis and to
301 better quantify the whole region of interest.
302 Due to logistical limitations, we performed the Ca^{2+} imaging for different
303 experimental groups on different days. In future work, we suggest that a final stimulated
304 Ca^{2+} spike could be used to normalize amplitudes, for example.

305 In the present study, for the primary cardiomyocytes, we performed mixed sex
306 cultures. Given the known sex differences in heart disease, the development of single
307 heart cultures may explain some differences between H9c2 cells and the models as H9c2
308 cells were isolated from a female left ventricle. Furthermore, the quantification of primary
309 cardiomyocyte culture composition may also explain differences if some cultures contain
310 more endothelial or fibroblast cells. And given the benefit of having a culture more
311 resembling what is seen *in vivo* it may be worthwhile to maintain the presence of
312 endothelial cells and fibroblasts. Finally, in future work, the sex of the animal from which
313 all heart tissues are derived should be recorded.
314
315 **Conclusions**
316 The H9c2 rat ventricular cardiomyoblast cell line has been used to model cardiomyocyte
317 development and disease. Here we quantified changes in three broad areas of H9c2 cell
318 biology across five and fourteen days of retinoic acid differentiation: morphology,
319 Ca^{2+}handling, and gene expression. Our quantitative assessment of shape, spontaneous
320 Ca^{2+}handling, and gene expression (both early at DIV5h and DIV3 as well as later at DIV14)
321 worked to address some of the knowledge gaps in the field to fully facilitate the use of
322 these cells. Depending on the context, we compared to DIV5 cells or primary
323 cardiomyocytes. Overall, we saw differentiation-induced changes in all three areas.
324 Increased cell size, multinucleation, development of spontaneous Ca^{2+} transients, and the
325 regulation of several key genes involved in these processes position H9c2 cells as a high-
326 throughput model for studying genetic and environmental factors affecting cardiomyocyte

327 biology, with the advantage of easier and shorter culturing protocols. Additionally, their
328 ease of transfection allows for targeted investigation of specific genes and pathways, and
329 the impacts of variants on cardiomyocyte differentiation. Our comprehensive
330 characterization indicates that H9c2 cells are a useful model in investigating components
331 of cardiomyocyte differentiation and may be particularly useful for understanding disease
332 mechanisms and for screening potential therapeutic interventions. However, the
333 heterogenicity of differentiated H9c2 cell analysis should take into account the spread of
334 differentiated cells and the addition of other models such as primary cardiomyocytes and
335 iPSC-derived cardiomyocytes may be of value to validate the findings.
336

337 **Materials and Methods**

338 All data that support the findings of this study are available from corresponding
339 authors upon reasonable request.

340 **Cell culture**

341 The H9c2 rat ventricular-derived cardiomyoblast cell line was obtained from the
342 American Type Culture Collection (ATCC, CRL-1446). H9c2 cells were cultured in
343 Dulbecco's Modified Eagle Medium (DMEM, ATCC, 30-2002) supplemented with 10% fetal
344 bovine serum (FBS) (Thermo Fisher, 12483020, reserve 10498874), 100 U/mL penicillin,
345 and 100 µg/mL streptomycin (Thermo Fisher, 15140122) at 37°C in 5% CO_2. Cells were
346 kept at or below 15 passages and passaged at 70-80% confluence to prevent the loss of
347 differential potential. Each vial was tested for mycoplasma contamination using the
348 universal mycoplasma detection kit (ATCC, 30-1012K).

349 H9c2 cells were differentiated as previously described [1]. Briefly, cells to be
350 collected within 5 days were seeded at 8,333 cells/cm^2 for RT-qPCR, Western blotting, and
351 live cell Ca^{2+} imaging experiments, and 8,000 cells/cm^2 for immunocytochemistry
352 experiments. For cells collected at 14 days, cell densities were decreased by half to
353 prevent cells from becoming confluent and detaching. One day after seeding, FBS was
354 decreased from 10% to 1% and media was supplemented with 1 μM all-trans retinoic acid
355 (ATRA) (Sigma, R2625-50MG). ATRA was added daily, in the dark, and cells were collected
356 prior to ATRA treatment (DIV0), at 5 hours (DIV5h), 3 days (DIV3), 5 days (DIV5), and 14 days
357 (DIV14) post ATRA treatment. Sample size was chosen based from the resource equation
358 [29].
359 One day after seeding, cells were transfected with a tetracycline inducible pCMB6-
360 AC-GFP-rtTA plasmid (Origene, PS100125) using jetPEI (Figure S2). 4 μL of jetPEI diluted in
361 150 mM NaCl was added to 2 μg of plasmid DNA also diluted in 150 mM NaCl, the mixture
362 was incubated for 15 minutes, and then added dropwise to the cells in DMEM containing
363 no antibiotics. One day after transfection, media was changed to DMEM containing 1%
364 FBS, 100 U/mL penicillin, and 100 μg/mL streptomycin, and was treated daily with 1 μM
365 ATRA. To induce GFP expression, 10 ng/mL Doxycycline hyclate (Sigma, D9891-1G) was
366 added to the differentiation media.
367 **Experimental Animals**
368 All animal procedures were approved by the University of Victoria Animal Care
369 Committee and performed in accordance with the guidelines set by the Canadian Council
370 on Animal Care. Male and female embryonic day (E)15.5– postnatal day (P)2 mice were

371 used in this study. C57BL/6J mice were obtained from The Jackson Laboratory (#000664).
372 Mice were housed under a 12/12 hour light/dark cycle starting at 8 A.M., with food and
373 water ad libitum; temperature was maintained between 20°C and 25°C and humidity at 40–
374 65%. Sample size was chosen based from the resource equation [29].
375
376 **Heart Tissue Extraction**
377 E15.5 and P2 heart tissue was flash frozen in liquid nitrogen and stored at -80°C.
378 E15.5 heart tissue intended for RNA analysis was stored in RNAlater Stabilization Solution
379 (Thermo Fisher, AM7020). Heart tissue was homogenized in a Dounce homogenizer on ice
380 with either 100 µL TRIzol (Thermo Fisher, 15596026) per 5-10 mg tissue (RNA) or RIPA lysis
381 buffer (9.1 mM PBS, 150 mM NaCl, 1.7 mM monobasic sodium phosphate, 9.1 mmol/L
382 dibasic sodium phosphate, 1% Igepal, 0.5% w/v sodium deoxycholate, 0.1% sodium
383 dodecyl sulphate (SDS), 10 µL/mL protease inhibitor cocktail (Sigma, P8340-5ML))
384 (protein). RNA was extracted from tissue samples after incubating on ice for 5 minutes and
385 then stored in TRIzol at -80°C. Protein lysates were pushed through a 27 ½ gauge needle 2
386 times and incubated on ice for 30 minutes; samples were then centrifuged at 13500 x g for
387 20 minutes at 4°C and the supernatant was also frozen at -80°C.
388
389 **Primary culture isolation**
390 Mouse cardiomyocytes were isolated according to standard methods previously
391 described [30]. 6-10 hearts were used per each given culture, representing 1 biological
392 replicate (N). Briefly, hearts were extracted from P1-P2 mice and transferred into

393 phosphate-buffered saline solution (without Ca^{2+} or Mg^{2+}) containing 20 mM 2,3-
394 Butanedione monoxime (BDM) (Sigma, B0753). In a sterile cell culture hood, the hearts
395 were washed, minced, and submerged in isolation medium consisting of Hanks' Balanced
396 Salt Solution (HBSS) with 20 mM BDM and 0.025% Trypsin (Gibco, 15090-046) for
397 incubation overnight under gentle agitation at 4°C. After incubation, the isolation medium
398 was removed, and the tissue was oxygenated in Leibovitz's L-15 medium containing 10 mM
399 BDM and 0.75 mg/ml of Collagenase/Dispase® mixture (Roche, 10269638001), then placed
400 in a shaking incubator for 30 minutes at 37°C. To release cells into suspension, the tissue
401 fragments were gently triturated and filtered through a 100 µm nylon mesh cell strainer.
402 Cells were centrifugated at 200 x g for 5 minutes to remove fibroblasts and endothelial
403 cells. The resulting pellet was resuspended in Dulbecco's modified Eagle's medium
404 (DMEM) supplemented with 5% Heat Inactivated Horse Serum (Thermo Fisher, 26050070)
405 and plated in a cell culture dish (a pre-plating step that removes many of the remaining
406 fibroblasts and endothelial cells). After a 2-3 hour incubation, non-adherent
407 cardiomyocytes were collected and plated on pre-coated collagen coverslips (Neuvitro,
408 NEU-GG-12-1.5-COLLAGEN) or onto collagen from calf skin (Fisher, ICN16008410) coated
409 35 mm glass bottom imaging dishes at a density of 1.5×10^5 cells per cm^2. The following
410 day, plating medium was replaced by DMEM containing 5% HIHS, 100 U/mL penicillin, and
411 100 µg/mL streptomycin for maintenance.
412
413
414 **Immunocytochemistry**

415 H9c2 cells were seeded onto fibronectin coated coverslips either purchased from
416 Neuvitro (NEU-GG-12-1.5-FIBRONECTIN) or coated in lab using fibronectin bovine plasma
417 (Sigma, F1141-1MG). Coverslips were fixed with 4% paraformaldehyde for 5 minutes at
418 DIV0, DIV5, and DIV14, followed by three washes with PBS containing Ca^{2+} or Mg^{2+}. Cells
419 were permeabilized with 0.1% Tween-20 for 5 minutes, washed three times in PBS as
420 before, blocked with 1% BSA and 22.52 mg/mL glycine in PBS-T, and then were incubated
421 with Hoechst (1:500) and phalloidin (1:500; 555, Invitrogen, A34055; Acti-Stain 670,
422 Cytoskeleton, PHDN1) diluted in 1% BSA in PBS overnight at room temperature for 1 hour.
423 Following secondary incubation, coverslips were washed three additional times, and
424 mounted with ProLong Gold Antifade Mountant (Thermo Fisher, P10144).
425 For transfected cells, fixation with 4% paraformaldehyde was performed as
426 previously described, followed by three washes in dPBS and mounting with ProLong Gold
427 Antifade Mountant.
428
429 **Microscopy**
430 Cells were imaged using a Leica TCS SP8 confocal microscope with HyD detectors. For
431 DIV0 versus DIV5 comparisons, imaging was performed using a 40X oil-immersion
432 objective set at 0.75 zoom (1.30 NA, pinhole = 65.28 µm, 3904 x 3904 (pixel size = 74.46 x
433 74.46 nm)). For DIV5 versus DIV14 cells, images were acquired using the 20X dry-objective
434 (0.7 NA, pinhole = 60.69 µm, 3800 x 3800 (pixel size =148.92 nm x 148.92 nm)).

435 For transfected cells, images were acquired using the 40X oil-immersion objective
436 set at 0.75 zoom (1.30 NA, pinhole = 65.08 μm, 2048 x 2048 (pixel size = 141.98 nm x
437 141.98 nm)). GFP was excited using the 488 nm Argon laser at 10% intensity.
438 STED images were acquired using a 100X oil-immersion objective (1.40 NA, pinhole
439 = 117.5 μm, pixel size optimized to 20 μm x 20 μm) at a zoom of 2. Phalloidin 555 was
440 excited using the 514 Argon laser at 20% intensity. Fluorescence was captured using the
441 HyD detector using the 660 STED laser at 25% 3D, 80% intensity and 70-90% power.
442 For all images presented, brightness and contrast were uniformly adjusted for
443 presentation purposes.
444
445 **Morphology Analysis**
446 To analyze morphological features of H9c2 cells, a custom Matlab script was
447 created: Morphology Analysis Overview A (code available at
448 https://github.com/SwayneLab/Quantification-of-H9c2-cell-differentiation-/). Images
449 were blinded before analysis. First, the analysis region for each cell was marked by
450 manually drawing a polygon around it. The script processed a binarized image where cell
451 pixels are set to one and background pixels to zero. Zeros were padded around the image
452 to ensure accurate boundary detection at the edges. The cell boundary was identified by
453 examining each pixel and its eight surrounding neighbours in a three x three grid, with
454 boundary pixels identified whenever a surrounding pixel was zero. Next, a covariance
455 matrix was created from these repositioned coordinates. An eigenvalue decomposition
456 was performed on this matrix to find the principal directions in which the cell extended.

457 These principal directions correspond to the longest (major) and shortest (minor)
458 dimensions of an ellipse that could fit around the cell.
459 Length, area, and eccentricity were calculated by first finding the center point, or
460 centroid, of each cell, averaging the positions of all the pixels that made up the cell. This
461 average point helped reposition the cell's pixel distribution to the center of the coordinate
462 system for easier analysis. Length was calculated from the square root of the largest
463 eigenvalue (major axis) and eccentricity was calculated from the ratio of largest eigenvalue
464 (major axis) to smallest eigenvalue (minor axis). The perimeter was calculated by counting
465 the number of boundary pixels, and area was calculated from filling in pixel area between
466 the boundary pixels. The number of nuclei per analyzed cell was calculated manually. All
467 plots and statistics were performed in Prism 10 for Mac OS X (version 10.3.1, GraphPad
468 Software, Inc.).
469
470 **Calcium imaging and analysis**
471 Isolated mouse cardiomyocytes seeded in collagen-coated 35 mm glass bottom imaging
472 dishes (ibidi, 81218-200) were loaded with cell-permeant 4 μM Fluo-4 AM (Invitrogen, F-
473 14201) for 35 minutes. H9c2 cells seeded in fibronectin-coated imaging dishes (ibidi,
474 81218-200) were loaded with 1.5 μM Fluo-4 AM at room temperature for 25 minutes.
475 Incubation time, temperature, and loading concentrations were optimized for each cell
476 type to prevent dye toxicity and compartmentalization. The cells were subsequently
477 washed using HBSS with 10 mM HEPES (Stem Cell Technologies, 37150) and incubated for
478 20 minutes to allow for de-esterification of the AM esters. All samples were imaged in

479 complete FluoroBrite™ DMEM media (Gibco™, A1896701) at 37°C and 5% CO_2 in a Tokai Hit
480 Stage Top Incubation System mounted on the Leica SP8. Fluo-4 was excited with the 488
481 nm argon laser line at 20% intensity through a 20x objective (0.70 NA, pinhole =242.65 µm).
482 Using the Leica SP8 resonant scanner, cardiomyocytes were imaged at 27.7 FPS for 1
483 minute and H9c2 cells were imaged at 14.6 FPS for 2 minutes. A minimum of 2 dishes were
484 imaged per biological replicate with 2-5 fields of view captured per dish.
485 Imaging files were initially processed by EZcalcium, an open-source, automated data
486 analysis package [31]. Part of the Matlab-based toolbox, the automated ROI detection
487 module was run first to detect all active cells, followed by the ROI refinement module to
488 semi-automatically eliminate dying cells and those with a poor signal/noise. Minor
489 movement artefacts in some FOV were not deemed significant by the motion correction
490 module. For quantification of the extracted data files, a series of Matlab scripts based on
491 those published [20] were employed. All data were analyzed and plotted in Prism 10 for
492 Mac OS X (version 10.3.1, GraphPad Software, Inc.), frequency distributions were created
493 in R (version 4.4.0).
494
495 **RNA extraction**
496 RNA was isolated using TRIzol as in [32]. Briefly, RNA from H9c2 cells or primary
497 cardiomyocytes was collected by adding 0.4 mL TRIzol per $1x10^5$-$1x10^7$ cells. Extracted
498 RNA was stored at -80°C.
499 RNA integrity was checked using the Agilent RNA 6000 Nano Kit (Agilent, 5067-
500 1511). Briefly, to minimize secondary structure, 2 µL RNA was denatured at 70°C for 2 min.

501 1 µL was loaded into the primed chip containing the gel-dye mix and RNA 6000 nano
502 marker. Once loaded, the chip was vortexed at 2400 rpm for 60 sec in the IKA vortex mixer,
503 loaded into the Agilent 2100 bioanalyzer, and the total RNA (eukaryotic) run was started
504 within 5 minutes. The RNA integrity number (RIN) scores were above 8.8 for H9c2 samples,
505 7.6 for P2 heart tissue and primary cardiomyocytes, and 1.5 for the E15.5 sample which
506 showed both the 18S and 28S bands.
507
508 **RT-qPCR**
509 1000 ng of RNA underwent treatment with DNase1 (Thermo Fisher, EN0521) to
510 digest any potential double-stranded DNA isolated with the RNA. cDNA was synthesized
511 from 500 ng of the DNase1 treated RNA using the Maxima First Strand cDNA Synthesis Kit
512 using random primers (Thermo Fisher, K1652). For each RT+ reaction, an RT- reaction was
513 also run. A GAPDH PCR reaction was run to confirm the cDNA synthesis and validate the
514 RT- controls on a 2% agarose gel. qPCR reactions for genes of interest were performed on a
515 QIAquant 96 well 5 plex qPCR machine (Qiagen, 9003010). Using PrimeTime qPCR probe
516 assays (IDT) and PrimeTime gene expression master mix (IDT, 1055772), 100 µg of RNA was
517 run in 10 µL reactions. The probe assays used are listed in Table S2. Standard cycling
518 conditions were run: polymerase activation at 95°C for 3 minutes, followed by 45 cycles of
519 denaturation at 95°C for 15 seconds and annealing/extension at 60°C for 1 minute. RT-
520 qPCR data was inputted into geNorm to determine the best normalization strategy [33]. To
521 normalize target genes, relative expression was calculated using the geometric mean of

522 two housekeeping genes, *Polr2a* and *Ppia*. Graphs were created in Prism 10 for Mac OS X
523 (version 10.3.1, GraphPad Software, Inc.).
524
525 **Western Blotting**
526 Adhered cells were washed 2 times in dPBS and lysed in RIPA lysis buffer (9.1 mM
527 PBS, 150 mM NaCl, 1.7 mM monobasic sodium phosphate, 9.1 mmol/L dibasic sodium
528 phosphate, 1% Igepal, 0.5% w/v sodium deoxycholate, 0.1% sodium dodecyl sulphate
529 (SDS), 10 µL/mL protease inhibitor cocktail (Sigma, P8340-5ML)) by scraping cells off the
530 plate or coverslip on ice. Cell lysates were then treated as described for the mouse heart
531 tissue. Protein content was determined using the DC protein assay (Bio-rad, 5000112). 10
532 µg of protein was incubated in Laemmli sample buffer (1X: 0.08 mM bromophenol blue,
533 0.05 M Tris-HCl pH 6.8, 0.058 M SDS, 3.33% v/v glycerol) at room temperature under
534 reducing conditions (5% dithiothreitol (DTT) and 5% β-mercaptoethanol), separated by
535 SDS-PAGE on TGX-stain free gels (Bio-rad, 4561094) and transferred to either a 0.2 µm
536 pore PVDF membrane (Bio-rad, 1620177) for peroxidase detection using the Syngene
537 G:Box imager or a 0.45 µm pore LF-PVDF membrane (Sigma, IPFL00010) for fluorescent
538 detection using the Licor Odyssey CLx Imager. For Western blots using the peroxidase-
539 based detection, the membrane was blocked with 5% fat free instant skim milk in TBS-T,
540 then incubated with indicated antibodies in the blocking solution, and protein bands were
541 visualized using the Clarity Western enhanced chemiluminescence substrate (Bio-Rad,
542 1705061). For Western blots using the fluorescent-based detection, the membrane was
543 blocked with intercept (TBS) blocking buffer (Li-cor, 927-60003), incubated with indicated

544 antibodies in the blocking solution containing 0.1% Tween 20 and 0.01% SDS (secondary
545 only). All proteins were normalized to total protein using Ponceau S Solution (0.1% w/v in
546 5% acetic acid) (Sigma, P7170-1L) or the Revert 700 Total Protein Stain (Li-cor, 926-11010)
547 and quantified with ImageJ. The antibodies and concentrations used are listed in Table S3.
548 Graphs were created in Prism 10 for Mac OS X (version 10.3.1, GraphPad Software, Inc.).
549

550 **Acknowledgements**

551 This work was supported by a Canadian Institutes for Health Research Project Grant
552 (CIHR; PJT-169064) awarded to LTA and LAS as well as from CIHR grants (PJT-185887, PJT-
553 189953) awarded to LAS. NY was supported by a Vanier Canada Graduate Scholarship
554 (Canadian Institutes of Health Research Vanier) and University of Victoria Donor Awards.
555 We acknowledge that this research was conducted on the traditional territory of the
556 Lək̓ʷəŋən (Songhees and Esquimalt) Peoples, and the Lək̓ʷəŋən and W̱SÁNEĆ Peoples
557 whose historical relationships with the land continue to this day. We also acknowledge the
558 Gitxsan peoples and their leadership as this work was initiated for and is foundational for
559 our ongoing research partnership on the mechanisms of inherited cardiac disease. The
560 progress of this work has been presented at in-person community gatherings, and virtually
561 by NY.
562

563 **Author contributions**

564 NY, JR, LA, and LAS conceived and designed the experiments. NY conducted the cell
565 culture work, morphological imaging, and biochemical assays, as well as advised in the

566 morphological and Ca^{2+} analyses. MRM created the morphological analysis, which both
567 MRM and RS conducted, NY then graphed and analyzed. JR and NY isolated primary
568 cardiomyocyte cultures. JR performed all Ca^{2+} imaging and analysis, as well as directed the
569 creation and statistical analysis for Figure 3. NY conducted all statistical analysis. NY and
570 KWLF created all figures. NY, JR, RS, KWLF, LEWS, LA, and LAS wrote and edited the
571 manuscript.
572

573 **References**

574 [1] C. Ménard, S. Pupier, D. Mornet, M. Kitzmann, J. Nargeot, P. Lory, Modulation of L-
575 type calcium channel expression during retinoic acid- induced differentiation of H9C2
576 cardiac cells, Journal of Biological Chemistry 274 (1999) 29063–29070.
577 https://doi.org/10.1074/jbc.274.41.29063.
578 [2] A.F. Branco, S.P. Pereira, S. Gonzalez, O. Gusev, A.A. Rizvanov, P.J. Oliveira, Gene
579 expression profiling of H9c2 myoblast differentiation towards a cardiac-like phenotype,
580 PLoS ONE 10 (2015) e0129303. https://doi.org/10.1371/journal.pone.0129303.
581 [3] C. Kankeu, K. Clarke, D. Van Haver, bcd Kris Gevaert, bc Francis Impens, bcd
582 Anna Dittrich, H. Llewelyn Roderick, E. Passante, H.J. Huber, Quantitative proteomics and
583 systems analysis of cultured H9C2 cardiomyoblasts during differentiation over time
584 supports a “function follows form” model of differentiation, 14 (2018) 181.
585 https://doi.org/10.1039/c8mo00036k.
586 [4] B.W. Kimes, B.L. Brandt, Properties of a clonal muscle cell line from rat heart,
587 Experimental Cell Research 98 (1976) 367–381. https://doi.org/10.1016/0014-
588 4827(76)90447-X.
589 [5] J. Hescheler, R. Meyer, S. Plant, D. Krautwurst, W. Rosenthal, G. Schultz,
590 Morphological, biochemical, and electrophysiological characterization of a clonal cell
591 (H9c2) line from rat heart, Circulation Research 69 (1991) 1476–1486.
592 https://doi.org/10.1161/01.RES.69.6.1476.
593 [6] S.J. Watkins, G.M. Borthwick, H.M. Arthur, The H9C2 cell line and primary neonatal
594 cardiomyocyte cells show similar hypertrophic responses in vitro, In Vitro Cell Dev Biol
595 Anim 47 (2011) 125–131. https://doi.org/10.1007/s11626-010-9368-1.
596 [7] R.D. Harvey, J.W. Hell, CaV1.2 Signaling Complexes in the Heart, J Mol Cell Cardiol
597 58 (2013) 143–152. https://doi.org/10.1016/j.yjmcc.2012.12.006.
598 [8] C. Campero-Basaldua, J. Herrera-Gamboa, J. Bernal-Ramírez, S. Lopez-Moran, L.-
599 A. Luévano-Martínez, H. Alves-Figueiredo, G. Guerrero, G. García-Rivas, V. Treviño, The
600 retinoic acid response is a minor component of the cardiac phenotype in H9c2 myoblast

601 differentiation, BMC Genomics 24 (2023) 431. https://doi.org/10.1186/s12864-023-09512-
602 0.
603 [9] D. Avanzato, A. Merlino, S. Porrera, R. Wang, L.M. Munaron, D. Mancardi, Role of
604 calcium channels in the protective effect of hydrogen sulfide in rat cardiomyoblasts, Cell
605 Physiol Biochem 33 (2014) 1205–1214. https://doi.org/10.1159/000358690.
606 [10] X. Xu, L. Ruan, X. Tian, F. Pan, C. Yang, G. Liu, Calcium inhibitor inhibits high
607 glucose-induced hypertrophy of H9C2 cells, Mol Med Rep 22 (2020) 1783–1792.
608 https://doi.org/10.3892/mmr.2020.11275.
609 [11] A. Hirschy, F. Schatzmann, E. Ehler, J.-C. Perriard, Establishment of cardiac
610 cytoarchitecture in the developing mouse heart, Developmental Biology 289 (2006) 430–
611 441. https://doi.org/10.1016/j.ydbio.2005.10.046.
612 [12] P. Ahuja, P. Sdek, W.R. Maclellan, Cardiac Myocyte Cell Cycle Control in
613 Development, Disease and Regeneration, Physiol Rev 87 (2007) 521–544.
614 https://doi.org/10.1152/physrev.00032.2006.
615 [13] S.D. Lundy, W.-Z. Zhu, M. Regnier, M.A. Laflamme, Structural and Functional
616 Maturation of Cardiomyocytes Derived from Human Pluripotent Stem Cells, Stem Cells
617 Dev 22 (2013) 1991–2002. https://doi.org/10.1089/scd.2012.0490.
618 [14] M. Fritzsche, D. Li, H. Colin-York, V.T. Chang, E. Moeendarbary, J.H. Felce, E.
619 Sezgin, G. Charras, E. Betzig, C. Eggeling, Self-organizing actin patterns shape membrane
620 architecture but not cell mechanics, Nat Commun 8 (2017) 14347.
621 https://doi.org/10.1038/ncomms14347.
622 [15] Y.M. Shirai, T.A. Tsunoyama, N. Hiramoto-Yamaki, K.M. Hirosawa, A.C.E. Shibata, K.
623 Kondo, A. Tsurumune, F. Ishidate, A. Kusumi, T.K. Fujiwara, Cortical actin nodes: Their
624 dynamics and recruitment of podosomal proteins as revealed by super-resolution and
625 single-molecule microscopy, PLoS One 12 (2017) e0188778.
626 https://doi.org/10.1371/journal.pone.0188778.
627 [16] F. Carton, S. Casarella, D. Di Francesco, E. Zanella, A. D'urso, L. Di Nunno, L.
628 Fusaro, D. Cotella, M. Prat, A. Follenzi, F. Boccafoschi, Cardiac Differentiation Promotes
629 Focal Adhesions Assembly through Vinculin Recruitment, Int J Mol Sci 24 (2023) 2444.
630 https://doi.org/10.3390/ijms24032444.
631 [17] W.E. Louch, J.T. Koivumäki, P. Tavi, Calcium signalling in developing
632 cardiomyocytes: implications for model systems and disease, J Physiol 593 (2015) 1047–
633 1063. https://doi.org/10.1113/jphysiol.2014.274712.
634 [18] S. Seki, M. Nagashima, Y. Yamada, M. Tsutsuura, T. Kobayashi, A. Namiki, N. Tohse,
635 Fetal and postnatal development of Ca2+ transients and Ca2+ sparks in rat
636 cardiomyocytes, Cardiovascular Research 58 (2003) 535–548.
637 https://doi.org/10.1016/S0008-6363(03)00255-4.
638 [19] K.R. Gee, K.A. Brown, W.-N.U. Chen, J. Bishop-Stewart, D. Gray, I. Johnson,
639 Chemical and physiological characterization of fluo-4 Ca2+-indicator dyes, Cell Calcium
640 27 (2000) 97–106. https://doi.org/10.1054/ceca.1999.0095.
641 [20] Z. Sun, T.C. Südhof, A simple Ca2+-imaging approach to neural network analyses in
642 cultured neurons, J Neurosci Methods 349 (2021) 109041.
643 https://doi.org/10.1016/j.jneumeth.2020.109041.

[21] M. Colpan, J. Iwanski, C.C. Gregorio, CAP2 is a regulator of actin pointed end dynamics and myofibrillogenesis in cardiac muscle, Commun Biol 4 (2021) 365. https://doi.org/10.1038/s42003-021-01893-w.
[22] J. Grego-Bessa, P. Gómez-Apiñaniz, B. Prados, M.J. Gómez, D. MacGrogan, J.L. de la Pompa, Nrg1 Regulates Cardiomyocyte Migration and Cell Cycle in Ventricular Development, Circ Res 133 (2023) 927–943. https://doi.org/10.1161/CIRCRESAHA.123.323321.
[23] W. Fu, Q. Liao, Y. Shi, W. Liu, H. Ren, C. Xu, C. Zeng, Transient induction of actin cytoskeletal remodeling associated with dedifferentiation, proliferation, and redifferentiation stimulates cardiac regeneration, Acta Pharm Sin B 14 (2024) 2537–2553. https://doi.org/10.1016/j.apsb.2024.01.021.
[24] W. Luo, Z.Z. Lieu, E. Manser, A.D. Bershadsky, M.P. Sheetz, Formin DAAM1 Organizes Actin Filaments in the Cytoplasmic Nodal Actin Network, PLoS One 11 (2016) e0163915. https://doi.org/10.1371/journal.pone.0163915.
[25] S. Xia, Y.B. Lim, Z. Zhang, Y. Wang, S. Zhang, C.T. Lim, E.K.F. Yim, P. Kanchanawong, Nanoscale Architecture of the Cortical Actin Cytoskeleton in Embryonic Stem Cells, Cell Reports 28 (2019) 1251-1267.e7. https://doi.org/10.1016/j.celrep.2019.06.089.
[26] M. Scarselli, P. Annibale, A. Radenovic, Cell Type-specific β2-Adrenergic Receptor Clusters Identified Using Photoactivated Localization Microscopy Are Not Lipid Raft Related, but Depend on Actin Cytoskeleton Integrity, J Biol Chem 287 (2012) 16768–16780. https://doi.org/10.1074/jbc.M111.329912.
[27] M.L. McCain, K.K. Parker, Mechanotransduction: the role of mechanical stress, myocyte shape, and cytoskeletal architecture on cardiac function, Pflugers Arch - Eur J Physiol 462 (2011) 89–104. https://doi.org/10.1007/s00424-011-0951-4.
[28] W.J. Kowalski, F. Yuan, T. Nakane, H. Masumoto, M. Dwenger, F. Ye, J.P. Tinney, B.B. Keller, Quantification of Cardiomyocyte Alignment from Three-Dimensional (3D) Confocal Microscopy of Engineered Tissue, Microscopy and Microanalysis 23 (2017) 826–842. https://doi.org/10.1017/S1431927617000666.
[29] W.N. Arifin, W.M. Zahiruddin, Sample Size Calculation in Animal Studies Using Resource Equation Approach, Malays J Med Sci 24 (2017) 101–105. https://doi.org/10.21315/mjms2017.24.5.11.
[30] E. Ehler, T. Moore-Morris, S. Lange, Isolation and Culture of Neonatal Mouse Cardiomyocytes, J Vis Exp (2013) e50154. https://doi.org/10.3791/50154.
[31] D.A. Cantu, B. Wang, M.W. Gongwer, C.X. He, A. Goel, A. Suresh, N. Kourdougli, E.D. Arroyo, W. Zeiger, C. Portera-Cailliau, EZcalcium: Open-Source Toolbox for Analysis of Calcium Imaging Data, Front Neural Circuits 14 (2020) 25. https://doi.org/10.3389/fncir.2020.00025.
[32] P. Chomczynski, A reagent for the single-step simultaneous isolation of RNA, DNA and proteins from cell and tissue samples, Biotechniques 15 (1993) 532–534, 536–537.
[33] J. Vandesompele, K. De Preter, F. Pattyn, B. Poppe, N. Van Roy, A. De Paepe, F. Speleman, Accurate normalization of real-time quantitative RT-PCR data by geometric averaging of multiple internal control genes, Genome Biol 3 (2002) research0034.1-0034.11.

[34] O. Selmin, P.A. Thorne, P.T. Caldwell, P.D. Johnson, R.B. Runyan, Effects of trichloroethylene and its metabolite trichloroacetic acid on the expression of vimentin in the rat H9c2 cell line, Cell Biol Toxicol 21 (2005) 83–95. https://doi.org/10.1007/s10565-005-0124-3.

[35] J.E. Balmer, R. Blomhoff, Gene expression regulation by retinoic acid, Journal of Lipid Research 43 (2002) 1773–1808. https://doi.org/10.1194/jlr.R100015-JLR200.

[36] D. Wang, D. Zhao, Y. Li, T. Dai, F. Liu, C. Yan, TGM2 positively regulates myoblast differentiation via enhancing the mTOR signaling, Biochimica et Biophysica Acta (BBA) - Molecular Cell Research 1869 (2022) 119173. https://doi.org/10.1016/j.bbamcr.2021.119173.

[37] S. Schiaffino, A.C. Rossi, V. Smerdu, L.A. Leinwand, C. Reggiani, Developmental myosins: expression patterns and functional significance, Skeletal Muscle 5 (2015) 22. https://doi.org/10.1186/s13395-015-0046-6.

[38] M. Nemer, Genetic insights into normal and abnormal heart development, Cardiovascular Pathology 17 (2008) 48–54. https://doi.org/10.1016/j.carpath.2007.06.005.

[39] C. Cao, L. Li, Q. Zhang, H. Li, Z. Wang, A. Wang, J. Liu, Nkx2.5: a crucial regulator of cardiac development, regeneration and diseases, Front Cardiovasc Med 10 (2023) 1270951. https://doi.org/10.3389/fcvm.2023.1270951.

[40] S. Balasubramanian, S.K. Mani, H. Kasiganesan, C.C. Baicu, D. Kuppuswamy, Hypertrophic Stimulation Increases β-actin Dynamics in Adult Feline Cardiomyocytes, PLoS One 5 (2010) e11470. https://doi.org/10.1371/journal.pone.0011470.

[41] M. Suhaeri, R. Subbiah, S.Y. Van, P. Du, I.G. Kim, K. Lee, K. Park, Cardiomyoblast (H9c2) Differentiation on Tunable Extracellular Matrix Microenvironment, Tissue Engineering - Part A 21 (2015) 1940–1951. https://doi.org/10.1089/ten.tea.2014.0591.

[42] K.A. Taylor, D.W. Taylor, F. Schachat, Isoforms of α-Actinin from Cardiac, Smooth, and Skeletal Muscle Form Polar Arrays of Actin Filaments, J Cell Biol 149 (2000) 635–646.

[43] L.A. Swayne, N.P. Murphy, S. Asuri, L. Chen, X. Xu, S. McIntosh, C. Wang, P.J. Lancione, J.D. Roberts, C. Kerr, S. Sanatani, E. Sherwin, C.F. Kline, M. Zhang, P.J. Mohler, L.T. Arbour, A Novel Variant in the ANK2 Membrane-Binding Domain is Associated with Ankyrin-B Syndrome and Structural Heart Disease in a First Nations Population with a High Rate of Long QT Syndrome, Circ Cardiovasc Genet 10 (2017) e001537. https://doi.org/10.1161/CIRCGENETICS.116.001537.

[44] N.S. York, J.C. Sanchez-Arias, A.C.H. McAdam, J.E. Rivera, L.T. Arbour, L.A. Swayne, Mechanisms underlying the role of ankyrin-B in cardiac and neurological health and disease, Front Cardiovasc Med 9 (2022) 964675. https://doi.org/10.3389/fcvm.2022.964675.

[45] S.R. Cunha, P.J. Mohler, Ankyrin-based cellular pathways for cardiac ion channel and transporter targeting and regulation, Seminars in Cell and Developmental Biology 22 (2011) 166–170. https://doi.org/10.1016/j.semcdb.2010.09.013.

[46] C.F. Kline, J. Scott, J. Curran, T.J. Hund, P.J. Mohler, Ankyrin-B Regulates Cav2.1 and Cav2.2 Channel Expression and Targeting, J Biol Chem 289 (2014) 5285–5295. https://doi.org/10.1074/jbc.M113.523639.

[47] N. Chanthra, T. Abe, M. Miyamoto, K. Sekiguchi, C. Kwon, Y. Hanazono, H. Uosaki, A Novel Fluorescent Reporter System Identifies Laminin-511/521 as Potent Regulators of

Cardiomyocyte Maturation, Sci Rep 10 (2020) 4249. https://doi.org/10.1038/s41598-020-61163-3.

[48] M. Tsikitis, Z. Galata, M. Mavroidis, S. Psarras, Y. Capetanaki, Intermediate filaments in cardiomyopathy, Biophys Rev 10 (2018) 1007–1031. https://doi.org/10.1007/s12551-018-0443-2.

[49] I. Shiraishi, D.G. Simpson, W. Carver, R. Price, T. Hirozane, L. Terracio, T.K. Borg, Vinculin is an Essential Component for Normal Myofibrillar Arrangement in Fetal Mouse Cardiac Myocytes, Journal of Molecular and Cellular Cardiology 29 (1997) 2041–2052. https://doi.org/10.1006/jmcc.1997.0438.

[50] A. Pott, S. Bock, I.M. Berger, K. Frese, T. Dahme, M. Keßler, S. Rinné, N. Decher, S. Just, W. Rottbauer, Mutation of the Na+/K+-ATPase Atp1a1a.1 causes QT interval prolongation and bradycardia in zebrafish, Journal of Molecular and Cellular Cardiology 120 (2018) 42–52. https://doi.org/10.1016/j.yjmcc.2018.05.005.

[51] T. Desplantez, Cardiac Cx43, Cx40 and Cx45 co-assembling: involvement of connexins epitopes in formation of hemichannels and Gap junction channels, BMC Cell Biology 18 (2017) 3. https://doi.org/10.1186/s12860-016-0118-4.

[52] B. Delorme, E. Dahl, T. Jarry-guichard, I. Marics, J.-P. Briand, K. Willecke, D. Gros, M. Théveniau-Ruissy, Developmental regulation of connexin 40 gene expression in mouse heart correlates with the differentiation of the conduction system, Developmental Dynamics 204 (1995) 358–371. https://doi.org/10.1002/aja.1002040403.

[53] C.W. Lo, A. Wessels, Cx43 Gap Junctions in Cardiac Development, Trends in Cardiovascular Medicine 8 (1998) 264–269. https://doi.org/10.1016/S1050-1738(98)00018-8.

[54] F. Jiang, K. Yin, K. Wu, M. Zhang, S. Wang, H. Cheng, Z. Zhou, B. Xiao, The mechanosensitive Piezo1 channel mediates heart mechano-chemo transduction, Nat Commun 12 (2021) 869. https://doi.org/10.1038/s41467-021-21178-4.

[55] D. Douguet, A. Patel, A. Xu, P.M. Vanhoutte, E. Honoré, Piezo Ion Channels in Cardiovascular Mechanobiology, Trends in Pharmacological Sciences 40 (2019) 956–970. https://doi.org/10.1016/j.tips.2019.10.002.

[56] T.M. da C.S. Carvalho, S. Cardarelli, M. Giorgi, A. Lenzi, A.M. Isidori, F. Naro, Phosphodiesterases Expression during Murine Cardiac Development, Int J Mol Sci 22 (2021) 2593. https://doi.org/10.3390/ijms22052593.

[57] H. Aoyama, Y. Ikeda, Y. Miyazaki, K. Yoshimura, S. Nishino, T. Yamamoto, M. Yano, M. Inui, H. Aoki, M. Matsuzaki, Isoform-specific roles of protein phosphatase 1 catalytic subunits in sarcoplasmic reticulum-mediated Ca2+ cycling, Cardiovascular Research 89 (2011) 79–88. https://doi.org/10.1093/cvr/cvq252.

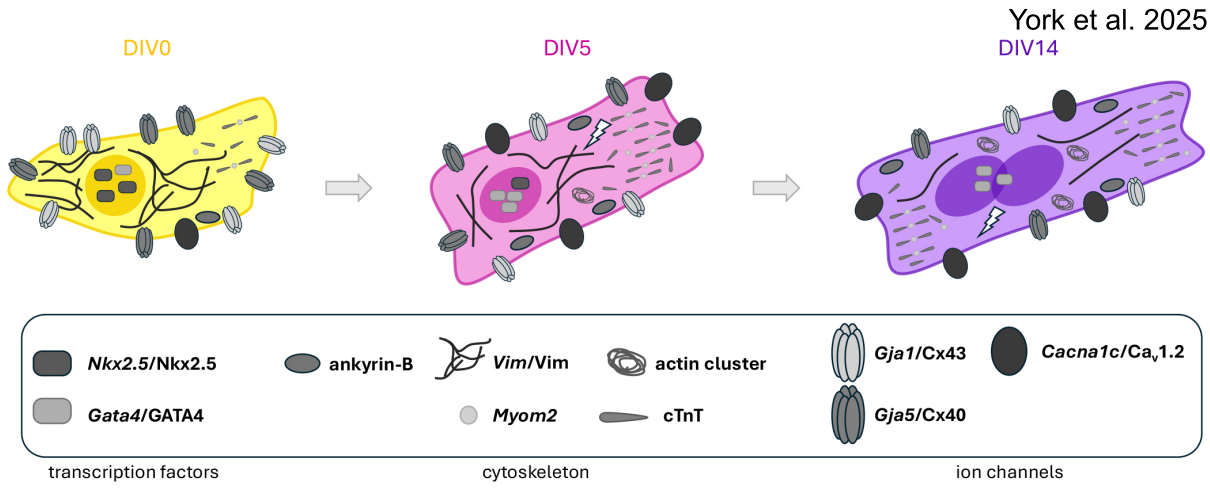

Figure 1. H9c2 cells display key markers of cardiomyocytes. H9c2 cells undergo a variety of genetic changes during H9c2 cell differentiation, upregulating key cardiomyocyte genes and proteins such as Cacna1c ($Ca_v1.2$), Tnnt2 (cTnT), and Myom2 (Myomesin-2).

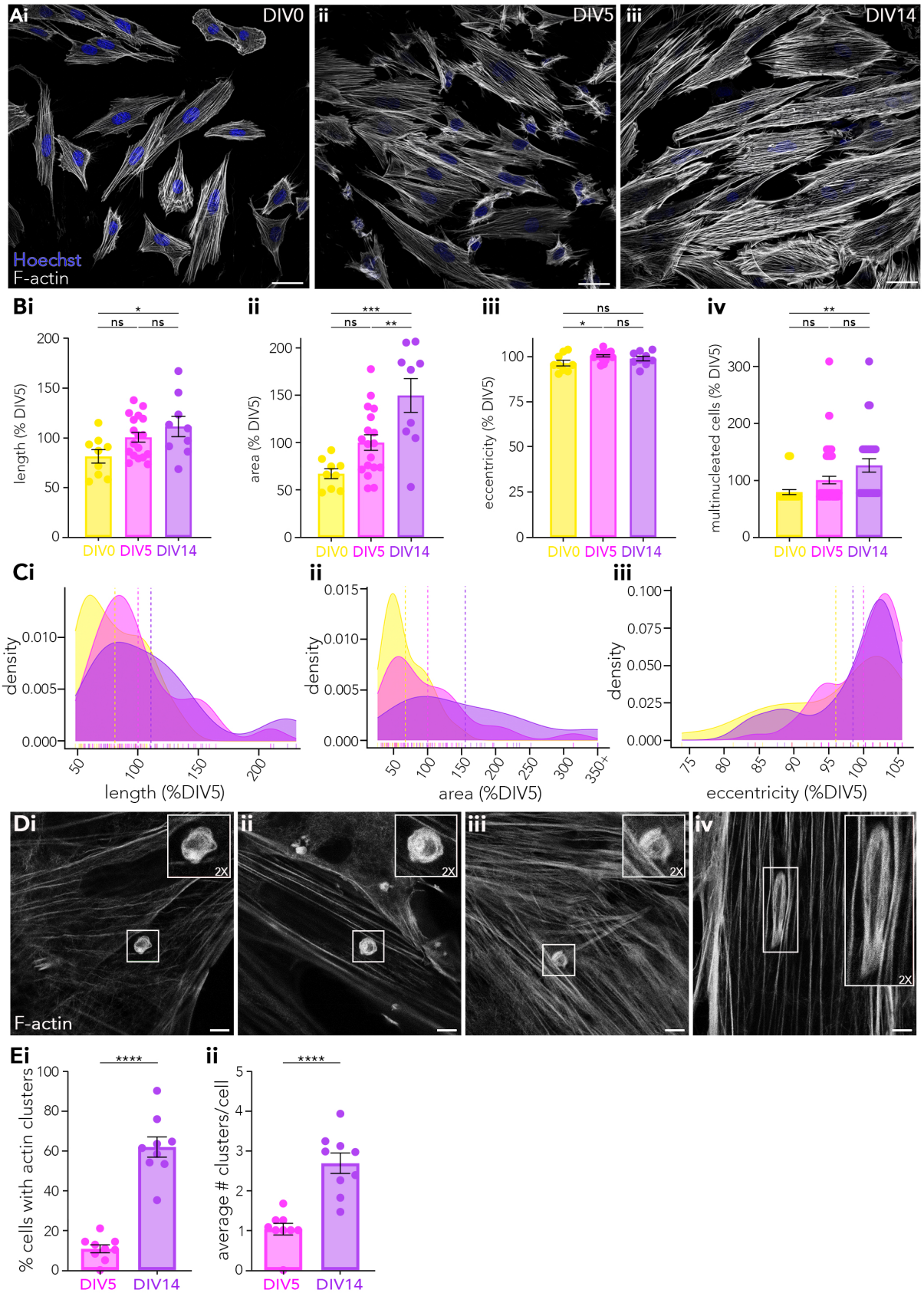
Ai
DIV0
ii
DIV5
iii
DIV14
Hoechst
F-actin
Bi
length (% DIV5)
DIV0 DIV5 DIV14
ii
area (% DIV5)
iii
eccentricity (% DIV5)
iv
multinucleated cells (% DIV5)
Ci
density
length (%DIV5)
area (%DIV5)
eccentricity (%DIV5)
Di
F-actin
2X
Ei
% cells with actin clusters
DIV5 DIV14
average # clusters/cell

773

774 *Figure 2. Differentiated H9c2 cells become larger, multi-nucleated, and develop localized actin intensities at DIV14.* H9c2
775 cell morphology at (Ai) DIV0, (Aii) DIV5, and (Aiii) DIV14 were analyzed using the F-actin stain Phalloidin (white) and nuclei
776 were counted via Hoechst staining (blue). Length, perimeter, area, eccentricity, and the number of nuclei per cell were
777 measured using a custom MATLAB script which resulted in significant increases in (Bi) length, (Bii) area, (Biii) eccentricity,
778 and (Biii) percentage of multinucleated cells. Density distribution plots show cell (Ci) length, (Cii) area, and (Ciii)
779 eccentricity at DIV5 display larger values than at DIV0. (Di-iii) Circular and (Div) elliptical actin-positive clusters were
780 present in many of the cells. Insets show STED resolved clusters at 2X magnification. (Ei) Quantification of the percent of
781 cells displaying actin clusters is higher at DIV14 than DIV5. (Eii) The number of actin clusters per cell also is increased at
782 DIV14. (B, E) Data is presented as mean ± SEM and (C) display probability density plots, indicating how likely a particular
783 value is to occur. Results are graphed as Yellow = DIV0, Magenta = DIV5, Purple = DIV14. (A) Scale bar = 40 μm. (D) Scale
784 bar = 5 μm, inlays were zoomed in by a factor of 2. N = 3 replicates, n = 27 cells for all groups (3 cells from each of the 3
785 FOV were selected). ****, $p < 0.0001$; ***, $p < 0.001$; **, $p < 0.01$; *, $p < 0.05$; ns, $p > 0.05$ by (B) one-way ANOVA and post-
786 hoc Tukey's multiple comparison and normalized to DIV5, or by (E) Independent T-test, see Table 1 for detailed statistics

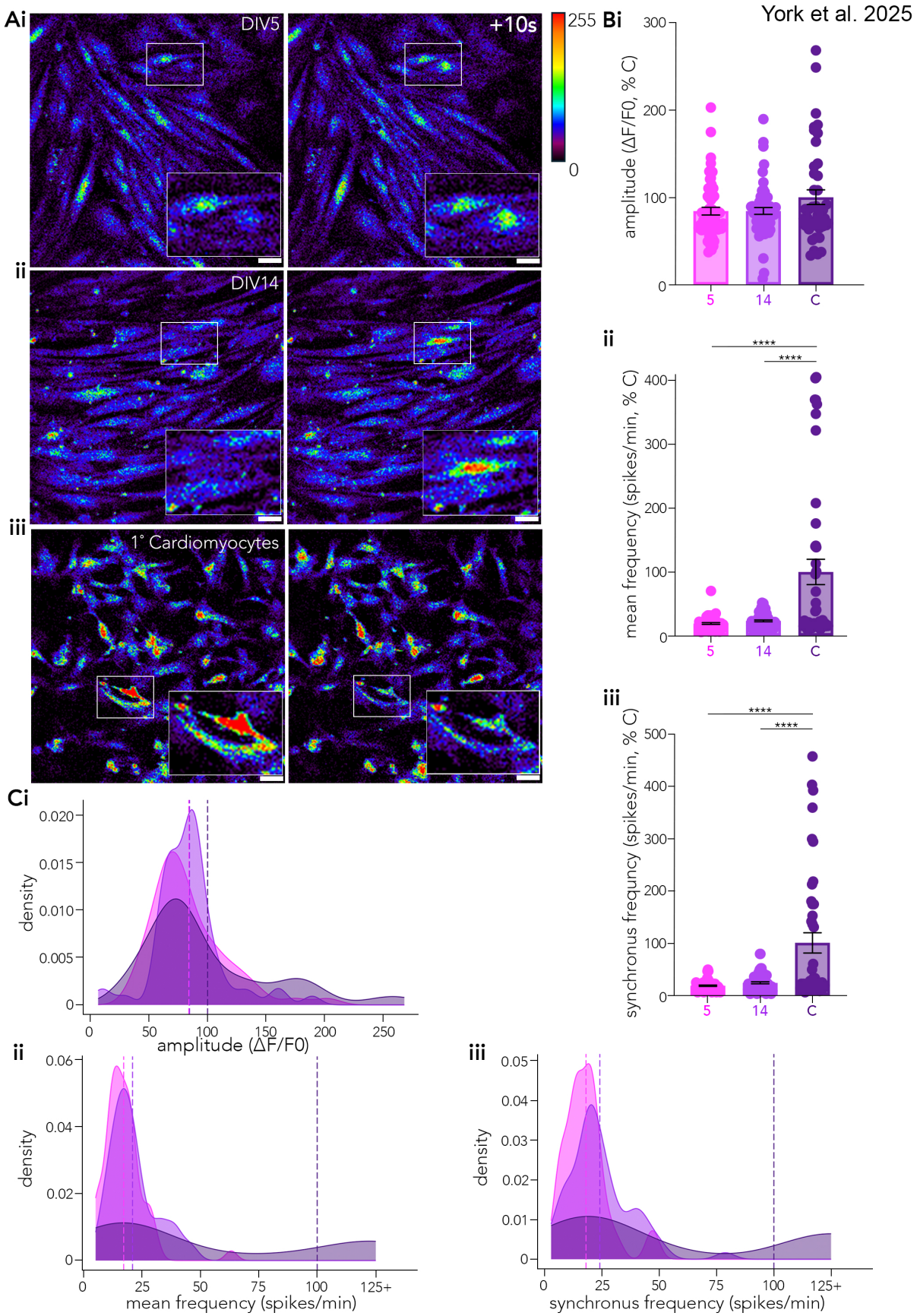
Ai
DIV5
+10s
255
0
ii
DIV14
iii
1° Cardiomyocytes
Bi
York et al. 2025
amplitude (ΔF/F0, % C)
300
200
100
0
5
14
C
ii
****
****
mean frequency (spikes/min, % C)
400
300
200
100
0
5
14
C
iii
****
****
synchronus frequency (spikes/min, % C)
500
400
300
200
100
0
5
14
C
Ci
density
0.020
0.015
0.010
0.005
0
0
50
100
150
200
250
amplitude (ΔF/F0)
ii
density
0.06
0.04
0.02
0
0
25
50
75
100
125+
mean frequency (spikes/min)
iii
density
0.05
0.04
0.03
0.02
0.01
0
0
25
50
75
100
125+
synchronus frequency (spikes/min)

787

788 *Figure 3 Differentiated H9c2 cells exhibit spontaneous Ca^{2+} transients, subpopulations of which exhibit characteristics*
789 *nearing those of primary cardiomyocytes.* Ca^{2+} imaging of differentiated H9c2 cells was performed using fluo-4 AM. Stills
790 10 seconds apart from 2 min (Ai) H9c2 DIV5, (Ai) H9c2 DIV14, or 1 min (Aii) primary cardiomyocytes time series show
791 spontaneous changes in $[Ca^{2+}]_i$. See supplemental Videos 1-3 for corresponding live imaging recordings. Inlays highlight
792 active cells in the field of view (FOV) undergoing a spike in $[Ca^{2+}]_i$. H9c2 cells have similar (Bi) spike amplitude to primary
793 cardiomyocytes while (Bii) frequency and (Biii) synchronous firing rate are significantly different. Density distribution
794 plots show the probability of a value in each group for (Ci) spike amplitude, (Cii) frequency, and (Ciii) synchronous firing
795 rate highlighting right shifts at DIV14 for (Cii) frequency and (Ciii) synchronous firing rate. DIV5 (N=56 FOV from 7
796 passages), DIV14 (N =60 FOV from 6 passages), primary cardiomyocytes (C; N = 43 FOV from 5 cultures). Data is
797 presented as mean ± SEM. Results are graphed as Magenta = DIV5, Purple = DIV14, Violet = C. Scale bar = 40 µm. ****, p
798 < 0.0001; unlabeled, $p > 0.05$ by one-way ANOVA and post-hoc Tukey's multiple comparison. Data is normalized to
799 primary cardiomyocytes, see Table 2 for detailed statistics.

York et al. 2025

Ai

retinoic acid signaling	transcription factors	cytoskeleton	ion channels/signal transduction
Rbp2	*Ctnnb1*, b-catenin	*Acta1*	*Atp1a1*
Tgm2	*Gata4*, **GATA4**	*Actb*, β-actin	***Cacna1c***
	Nkx2.5, **Nkx2.5**	**α-actinin**	*Gja1*, **Cx43**
		ankyrin-B	***Gja5***
		Myom2	*Piezo1*
		Tnnt2, **cTnT**	*Pde4a*
		Vim, **vimentin**	*Ppp1ca*
		vinculin	

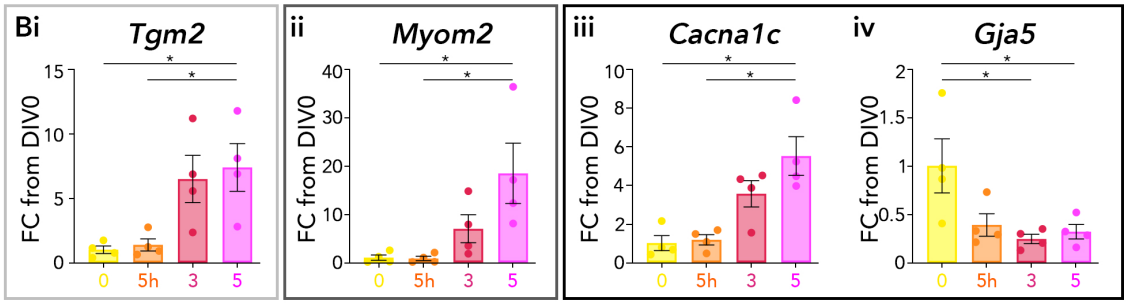

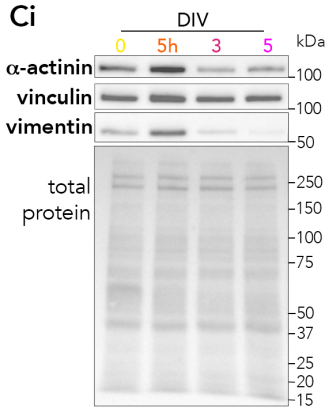

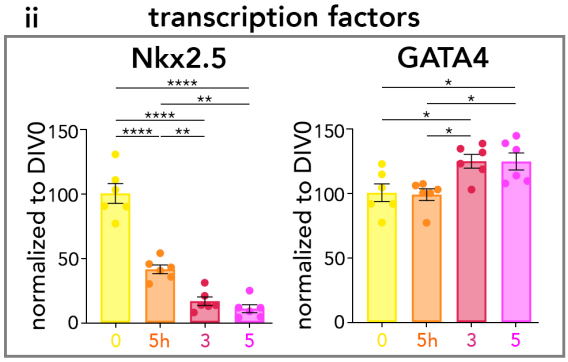

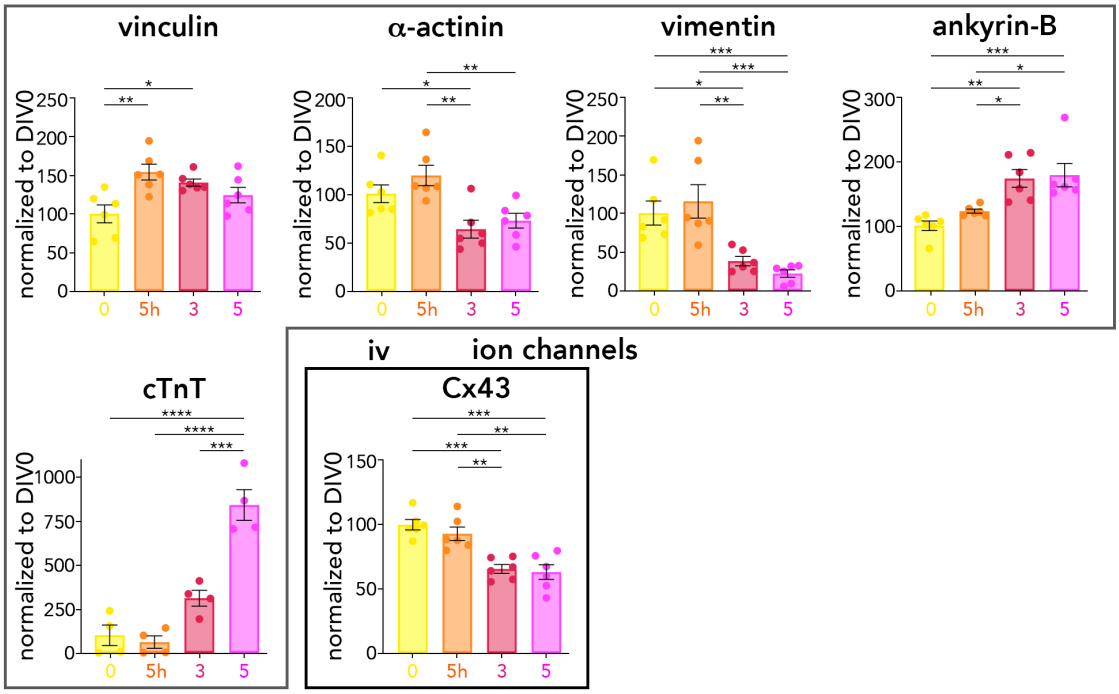

800

Figure 4. Differentiated H9c2 cells exhibit gene expression changes consistent with cardiomyocyte differentiation. (A) table of genes involved in retinoic acid signaling, transcription, cytoskeleton, ion flux regulation, and signal transduction were analyzed, bolded resulted in significant differences between groups. Transcript expression of (Bi) *Tgm2*, (Bii) *Myom2* and (Biii) *Cacna1c* increased during differentiation, while (Biv) *Gja5* decreased. (Ci) Representative western blot for some of the cytoskeletal proteins is shown. Protein expression of (Cii) transcription factor Nkx2.5 decreased while GATA 4 levels increased across differentiation. (Ciii) Cytoskeletal proteins levels increased and then returned to base line for vinculin, decreased for α-actinin and vimentin, and increased for ankyrin-B and cTnT. Lastly, (Civ) the ion channel Cx43 levels decreased during differentiation. For RT-qPCR data: DIV0, DIV5h, DIV3, DIV5 (N=4 passages). For western blot data, DIV0, DIV5h, DIV3, DIV5 (N=6 passages, except cTnT N=4 passages). Data is presented as mean ± SEM. Results are graphed as Yellow = DIV0, Orange = DIV5h, Red = DIV3, Magenta = DIV5. ****, $p < 0.0001$; ***, $p < 0.001$; **, $p < 0.01$; *, $p < 0.05$; unlabeled, $p > 0.05$ by one-way ANOVA and post-hoc Tukey's multiple comparison. Data is normalized to DIV0.

Ai

transcription factors	cytoskeleton	ion channels/signal transduction
Ctnnb1	**α-actinin**	*Atp1a1*
Nkx2.5, **Nkx2.5**	*Tnnt2*, **cTnT**	*Cacna1c*
	Vim, **vimentin**	*Cx43*
	vinculin	*Gja5*
		Piezo1

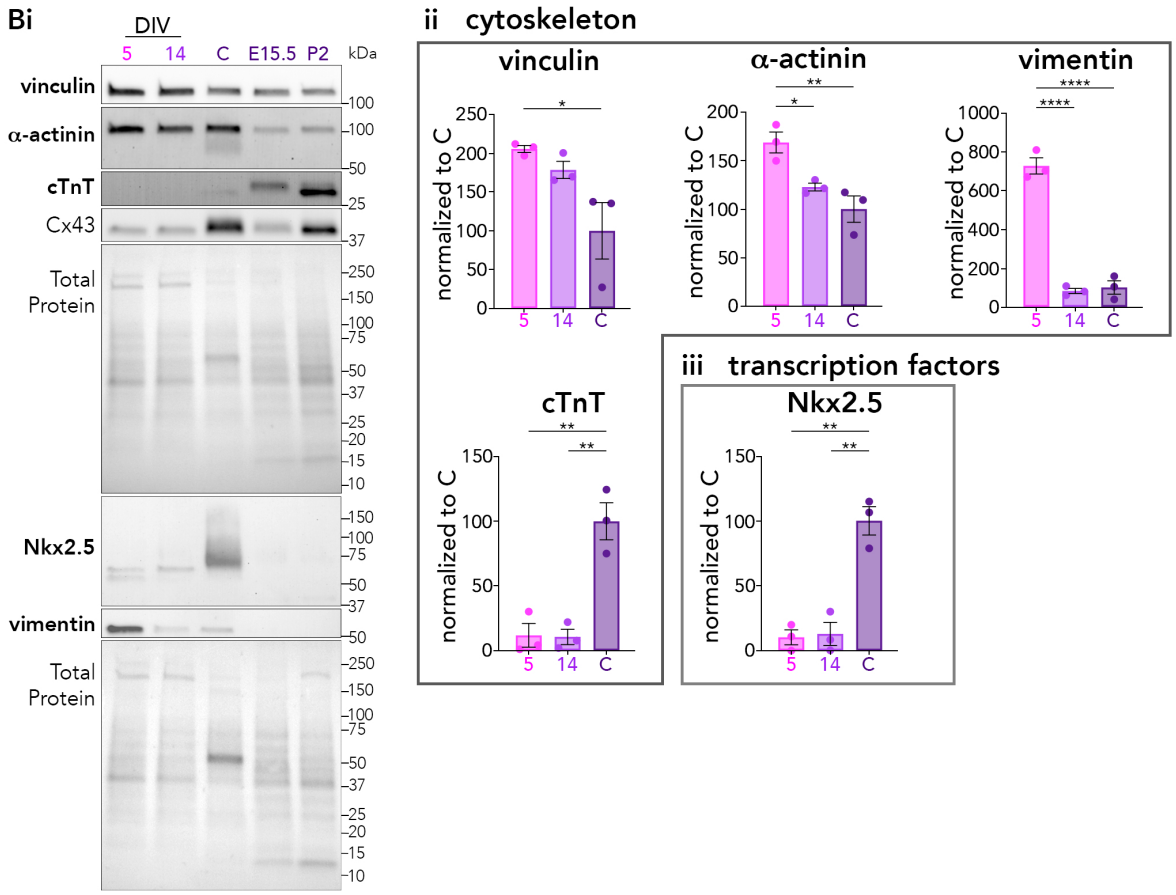

Figure 5.Differentiated H9c2 cells at DIV14 more closely resemble primary cardiomyocytes than DIV5. (A) table of genes involved in retinoic acid signaling, transcription, cytoskeleton, ion flux regulation, and signal transduction were analyzed, bolded resulted in significant differences between groups. (Bi) Representative western blot for some of the cytoskeletal proteins is shown. (Bii) Protein expression of several cytoskeletal proteins were significantly different at DIV5 but not at DIV14 including vinculin, α-actinin, and vimentin, while cTnT levels were significantly decreased at both DIV5 and DIV14 compared to primary cardiomyocytes. (Biii) Similarly, the levels of transcription factor Nkx2.5 were also significantly decreased at both DIV5 and DIV14 compared to primary cardiomyocytes. For western blot data DIV5, DIV14 (N = 3 passages; primary cardiomyocytes (C) (N = 3 cultures); P2, E15.5 (N=3 hearts). Data is presented as mean ± SEM. Results are graphed as Yellow = DIV0, Orange = DIV5h, Red = DIV3, Magenta = DIV5. ****, $p < 0.0001$; ***, $p < 0.001$; **, $p < 0.01$; *, $p < 0.05$; unlabeled, $p > 0.05$ by one-way ANOVA and post-hoc Tukey's multiple comparison. Data is normalized to primary cardiomyocytes (C).

826 **Table 1. Summary statistics of H9c2 cell morphology analysis results in significant**
827 **increases to length, area, eccentricity, and multinucleation across differentiation.**
828 Minimum (Min) and maximum (Max) values for each condition as well as the mean ±
829 SEM are listed. A one-way ANOVA was performed, if this provided a significant result,
830 then the Tukey multiple comparisons test was used to determine which groups were
831 significant. N=9 FOV for DIV0, DIV14, and N=18 FOV for DIV5 each from a total of 3
832 passages. All values are normalized to DIV5.

parameter	timepoint	min (%)	max (%)	mean ± SEM	p-value ANOVA	p-value Tukey		
						0-5	0-14	5-14
normalized length	DIV0	55.5	114.4	80.8% ± 6.7	0.0321 "*"	0.1258 "ns"	0.0278 "*"	0.5083 "ns"
	DIV5	72.9	137.1	100% ± 4.9				
	DIV14	68.1	166.3	110.7% ± 10.2				
normalized perimeter	DIV0	36.2	137.1	77.2% ± 10.5	0.2392 "ns"	0.3290 "ns"	0.2567 "ns"	0.9122 ns"
	DIV5	47.4	177.0	100% ± 8.5				
	DIV14	47.4	186.0	106.4% ± 16.3				
normalized area	DIV0	47.2	92.0	67.1% ± 5.3	0.0002 "***"	0.0934 "ns"	0.0001 "***"	0.0072 "**"
	DIV5	51.7	177.5	100% ± 8.3				
	DIV14	53.2	206.5	149.7% ± 17.9				
normalized eccentricity	DIV0	90.1	103.4	96.0% ± 1.6	0.0302 "*"	0.0231 "*"	0.3077 "ns"	0.5412 "ns"
	DIV5	94.6	105.2	100% ± 0.6				
	DIV14	91.5	103.4	98.5% ± 1.3				
normalized multinucleation	DIV0	71.1	142.1	79.0% ± 4.4	0.0018 "**"	0.1446 "ns"	0.0012 "**"	0.0578 "ns"
	DIV5	71.1	308.6	100% ± 6.5				
	DIV14	77.1	308.6	125.7% ± 11.8				

833

834 **Table 2. Summary statistics of H9c2 cell spontaneous calcium dynamics.** Minimum
835 (Min) and maximum (Max) values for each condition as well as the mean ± SEM are
836 listed for each parameter. DIV5 (N=56 FOV from 7 passages), DIV14 (N=60 FOV from 6
837 passages), primary cardiomyocytes (N=43 FOV from 5 cultures). A one-way ANOVA
838 was performed, if this provided a significant result, then the Tukey multiple
839 comparisons test was used to determine which groups were significant. All values are
840 normalized to primary cardiomyocytes (C).

parameter	timepoint	min (%)	ax (%)	mean ± SEM	p-value ANOVA	p-value Tukey		
						5-14	5-C	14-C
normalized amplitude	DIV5	37.1	202.3	84.1% ± 4.3	0.0789 "ns"	0.9999 "ns"	0.1138 "ns"	0.1099 "ns"
	DIV14	6.8	189.1	84.2% ± 3.9				
	C	33.4	267.6	100% ± 8.5				
normalized frequency	DIV5	6.0	70.4	19.3% ± 1.3	<0.0001 "****"	0.9413 "ns"	< 0.0001 "****"	< 0.0001 "****"
	DIV15	7.7	51.9	23.5% ± 1.4				
	C	8.9	404.8	100% ± 19.8				
normalized synchronous frequency	DIV5	5.4	48.9	18.0% ± 1.3	<0.0001 "****"	0.8639 "ns"	< 0.0001 "****"	< 0.0001 "****"
	DIV14	2.7	78.8	23.7% ± 1.7				
	C	5.4	456.5	100% ± 19.4				

841

842 **Table 3. H9c2 cell transcript levels of key cardiomyocyte cytoskeletal proteins and**
843 **ion channels increases over differentiation.** For DIV5, which was compared to DIV0,
844 and DIV5 and DIV14, which were compared to C, a one-way ANOVA was performed, if
845 this provided a significant result, then the Tukey multiple comparisons test was used to
846 determine which groups were significant. DIV0, DIV5h, DIV3, DIV5 (N=4 passages);
847 DIV14, primary cardiomyocytes, P2 (N=3 passages, cultures, hearts); E15.5 (N=1 heart).

Transcript	DIV	FC from DIV0	Log2	p-value ANOVA	p-value Tukey			previously reported
					vs 0h	vs 5h	vs 3d	
Rbp2	5h	0.68 ± 0.26	-0.90	0.1480 "ns"	0.9552 "ns"			↑ [2]
	3	1.82 ± 0.48	0.73		0.5781 "ns"	0.3142 "ns"		
	5	2.04 ± 0.57	0.87		0.3831 "ns"	0.1862 "ns"	0.9833 "ns"	
Tgm2	5h	1.38 ± 0.47	0.26	0.0082 "**"	0.9970 "ns"			↑ [8]
	3	6.49 ± 3.66	2.49		0.0548 "ns"	0.0771 "ns"		
	5	7.38 ± 3.70	2.71		0.0240 "*"	0.0340 "*"	0.9630 "ns"	
Myh2	5h	0.71 ± 0.17	-0.74	0.4557 "ns"	0.6888 "ns"			
	3	0.57 ± 0.20	-1.14		0.3966 "ns"	0.9520 "ns"		
	5	0.75 ± 0.13	-0.49		0.7787 "ns"	0.9984 "ns"	0.9010 "ns"	
Tnnt2	5h	1.35 ± 0.59	-0.04	0.0943 "ns"	0.9998 "ns"			↑ [2,8]
	3	9.89 ± 3.68	2.95		0.2675 "ns"	0.2978 "ns"		
	5	10.90 ± 5.33	2.86		0.1948 "ns"	0.2186 "ns"	0.9963 "ns"	
Ctnnb1	5h	0.97 ± 0.17	-0.11	0.7799 "ns"	0.991 "ns"			= [8]
	3	1.17 ± 0.25	0.14		0.9102 "ns"	0.8572 "ns"		
	5	1.17 ± 0.14	0.20		0.9040 "ns"	0.8497 "ns"	> 0.9999 "ns"	
Gata4	5h	0.79 ± 0.11	-0.39	0.5909 "ns"	0.9081 "ns"			= [8]
	3	0.79 ± 0.24	-0.58		0.9073 "ns"	> 0.9999		

						"ns"		
	5	0.56 ± 0.08	-0.89		0.5177 "ns"	0.8777 "ns"	0.8786 "ns"	
Nkx2.5	5h	1.18 ± 0.50	-0.39	0.1202 "ns"	0.9917 "ns"			
	3	1.55 ± 0.30	0.53		0.8317 "ns"	0.9412 "ns"		
	5	2.60 ± 0.65	4.99		0.1209 "ns"	0.1894 "ns"	0.4153 "ns"	
Actb	5h	0.96 ± 0.11	-0.08	0.2162 "ns"	0.9943 "ns"			↓ [8]
	3	0.85 ± 0.10	-0.26		0.7685 "ns"	0.8865 "ns"		
	5	0.62 ± 0.07	-0.73		0.2183 "ns"	0.3115 "ns"	0.6978 "ns"	
Myom2	5h	0.83 ± 0.46	-0.20	0.0115 "*"	> 0.9999 "ns"			↑ [2,8]
	3	6.95 ± 2.88	3.39		0.6266 "ns"	0.6060 "ns"		
	5	18.40 ± 6.22	4.99		0.0176 "*"	0.0166 "*"	0.1416 "ns"	
Vim	5h	1.28 ± 0.52	-0.10	0.3171 "ns"	0.9478 "ns"			↓ [8]
	3	0.65 ± 0.45	-1.00		0.9015 "ns"	0.6256 "ns"		
	5	0.32 ± 0.15	-2.48		0.5688 "ns"	0.2953 "ns"	0.9183 "ns"	
Atp1a1	5h	1.07 ± 0.23	-0.01	0.7603 "ns"	0.9975 "ns"			= [8]
	3	1.34 ± 0.29	0.31		0.7972 "ns"	0.8839 "ns"		
	5	1.28 ± 0.28	0.27		0.8664 "ns"	0.9353 "ns"	0.9988 "ns"	
Cacna1c	5h	1.17 ± 0.39	0.08	0.0010 "***"	0.9976 "ns"			↑ [8]
	3	3.54 ± 0.68	1.71		0.0690 "ns"	0.0943 "ns"		
	5	5.49 ± 1.0	2.39		0.0018 "**"	0.0024 "**"	0.1993 "ns"	
Gja1	5h	1.04 ± 0.12	0.03	0.8164 "ns"	0.9956 "ns"			= [8]
	3	1.10 ± 0.08	0.12		0.9517 "ns"	0.9905 "ns"		
	5	0.93 ± 0.18	-0.19		0.9752	0.9168	0.7862	

					"ns"	"ns"	"ns"	
Gja5	5h	0.39 ± 0.12	-1.52	0.0201 "*"	0.0745 "ns"			↓ [8]
	3	0.25 ± 0.05	-2.12		0.0243 "*"	0.9144 "ns"		
	5	0.32 ± 0.08	-1.76		0.0439 "*"	0.9893 "ns"	0.9859 "ns"	
Peizo1	5h	1.17 ± 0.33	0.05	0.3744 "ns"	0.9913 "ns"			
	3	1.53 ± 0.40	0.45		0.8017 "ns"	0.9241 "ns"		
	5	2.00 ± 0.58	0.81		0.3651 "ns"	0.5155 "ns"	0.8559 "ns"	
Pde4a	5h	0.97 ± 0.55	-0.60	0.6120 "ns"	> 0.9999 "ns"			↓ [2], = [8]
	3	0.46 ± 0.38	-1.42		0.8051 "ns"	0.8303 "ns"		
	5	0.36 ± 0.17	-1.85		0.7121 "ns"	0.7407 "ns"	0.9981 "ns"	
Ppp1ca	5h	0.99 ± 0.12	-0.05	0.9516 "ns"	> 0.9999 "ns"			= [8]
	3	0.97 ± 0.15	-0.09		0.9994 "ns"	0.9999 "ns"		
	5	0.88 ± 0.19	-0.31		0.9535 "ns"	0.9641 "ns"	0.9769 "ns"	

transcript	DIV	FC from C	Log2	p-value ANOVA	p-value Tukey		
					5-14	5-C	14-C
Tnnt2	5	0.04 ± 0.02	-5.29	0.3477 "ns"	0.9999 "ns"	0.4053 "ns"	0.4118 "ns"
	14	0.05 ± 0.03	-5.06				
Ctnnb1	5	0.06 ± 0.03	-4.63	0.0766 "ns"	>0.9999 "ns"	0.1071 "ns"	0.1054 "ns"
	14	0.06 ± 0.04	-5.02				
Nkx2.5	5	0.09 ± 0.07	-4.35	0.4550 "ns"	>0.9999 "ns"	0.5159 "ns"	0.5144 "ns"
	14	0.09 ± 0.04	-3.94				
Vim	5	1.89 ± 1.36	0.12	0.7564 "ns"	0.8031 "ns"	0.7829 "ns"	0.9992 "ns"
	14	1.05 ± 0.70	-0.59				
Atp1a1	5	0.18 ± 0.03	-2.52	0.2100	0.9999	0.2651	0.2604

	14	0.18 ± 0.04	-2.61	"ns"	"ns"	"ns"	"ns"
Cacna1c	5	0.12 ± 0.03	-3.14	0.0445 "*"	0.9886 "ns"	0.0592 "ns"	0.0709 "ns
	14	0.16 ± 0.05	-2.75				
Gja5	5	0.40 ± 0.20	-2.06	0.3337 "ns"	0.8982 "ns"	0.5305 "ns"	0.3240 "ns"
	14	0.17 ± 0.10	-3.09				
Peizo1	5	4.12 ± 1.88	1.92	0.1131 "ns"	0.6508 "ns"	0.3214 "ns"	0.1019 "ns"
	14	5.92 ± 2.06	2.35				

850 **Table 4. H9c2 cell protein levels of key cardiomyocyte cytoskeletal proteins and**
851 **cardiac markers increases over differentiation.** A one-way ANOVA was performed, if
852 this provided a significant result, then the Tukey's multiple comparisons test was used
853 to determine which groups were significant. DIV0, DIV5h, DIV3, DIV5 (N=6 passages,
854 except cTnT N=4 passages); DIV14, primary cardiomyocytes (C), P2, E15.5 (N=3
855 passages, cultures, hearts respectively).

protein	DIV	normalized percent to DIV0	p-value ANOVA	p-value Tukey			previously reported
				vs 0	vs 5h	vs 3	
Nkx2.5	5h	41.3% ± 3.4	<0.0001 "****"	<0.0001 "****"			
	3	16.6% ± 3.3		<0.0001 "****"	0.0078 "**"		
	5	10.9% ± 3.1		<0.0001 "****"	0.0011 "*"	0.8297 "ns"	
GATA4	5h	98.5% ± 4.5	0.0043 "**"	0.9979 "ns"			= [2]
	3	124% ± 5.3		0.0390 "*"	0.0267 "*"		
	5	124% ± 6.6		0.0409 "*"	0.0280 "*"	>0.9999 "ns"	
α-actinin	5h	119% ± 9.2	0.0013 "**"	0.4883 "ns"			
	3	63.5% ± 10.5		0.0487 "*"	0.0020 "**"		
	5	72.3 ± 7.6		0.1760 "ns"	0,0093 "**"	0.9050 "ns"	
Cx43	5h	92.9% ± 5.3	<0.0001 "****"	0.7108 "ns"			
	3	65.6% ± 3.4		0.0002 "***"	0.0028 "**"		
	5	63.1% ± 5.7		0.0001 "***"	0.0012 "**"	0.9807 "ns"	
cTnT	5h	61.3% ± 35.2	<0.0001 "****"	0.9666 "ns"			↑ [2,3]
	3	311% ± 44.9		0.1106 "ns"	0.0510 "ns"		
	5	839% ± 87.2		<0.0001 "****"	<0.0001 "****"	0.0002 "***"	
vinculin	5h	154% ± 10.2	0.0043 "**"	0.0033 "**"			↓ [3,34]
	3	141% ± 4.58		0.0314 "*"	0.7444 "ns"		
	5	124% ± 10.0		0.2952	0.1522	0.6297	

				"ns"	"ns"	"ns"
vimentin	5h	115% ± 21.5	0.0002 "***"	0.8661 "ns"		
	3	38.0% ± 6.0		0.0224 "*"	0.0040 "**"	
	5	21.9% ± 4.8		0.0036 "**"	0.0006 "***"	0.8425 "ns"
β-actin	5h	131% ± 14.0	0.0663 "ns"	0.4412 "ns"		
	3	149% ± 11.9		0.1076 "ns"	0.8139 "ns"	
	5	153% ± 13.1		0.0756 "ns"	0.7132 "ns"	0.9977 "ns"
ankyrin-B	5h	122.5 ± 3.1	0.0003 "***"	0.5575 "ns"		
	3	172.7 ± 13.7		0.0018 "**"	0.0352 "*"	
	5	177.9 ± 17.9		0.0009 "***"	0.0182 "*"	0.9896 "ns"

protein	DIV	normalized percent to C	p-value ANOVA	p-value Tukey		
				5-14	5-C	14-C
Nkx2.5	5	10.3% ± 5.7	0.0005 "***"	0.9758 "ns"	0.0009 "***"	0,0010 "**"
	14	12.9% ± 8.9				
α-actinin	5	169% ± 10.7	0.0085 "**"	0.0436 "*"	0.0075 "**"	0.3271 "ns"
	14	123% ± 4.0				
Cx43	5	41.5% ± 19.1	0.3558 "ns"	0.9895 "ns"	0.4522 "ns"	0.3878 "ns"
	14	35.2% ± 10.6				
cTnT	5	11.9 % ± 9.2	0.0013 "**"	0.9963 "ns"	0.0023 "**"	0.0022 "ns"
	14	10.7% ± 5.9				
vinculin	5	205% ± 4.5	0.0352 "*"	0.6801 "ns"	0.0344 "*"	0.1005 "ns"
	14	178% ± 11.0				
vimentin	5	725% ± 42.0	<0.0001 "****"	<0.0001 "****"	<0.0001 "****"	0.9229 "ns"